HTR-N

Work Package: 2	HTR-N project document No.: HTR-N-02/05-D-2.2.2				Q.A. level: 1
Task: 2.2.2	Document type: Deliverable				Document status: final
Issued by: IKE	original document No.:	Annex pg. 0	Rev. 0	Q.A. level B	Dissemination level:

Document Title

Synthesis on Requirements for Improvement of Nuclear Data

Author(s)

W. Bernnat, M. Mattes, J. Keinert

Organisation, Country

IKE, University of Stuttgart, Germany

Notes

Electronic filing: SINTER

Electronic file format: Microsoft Word 97/ Adobe PDF

1	20.10.2004	Final issue				
0	15.03.2003	first issue			IKE W. Bernnat	FZJ W. von Lensa
Rev.	**Date**	**Short Description**	**Prepared by**	**Partners' Review**	**Control WP Manager**	**Approval Project Manager**

Chronology and history of revisions

Rev.	Date	Description
0	15.03.2003	First issue
1	20.10.2004	Final issue

DISTRIBUTION

EXTERNAL (SINTER database)

HTR-N Partners
HTR-N Coordinator (3 printed copies)

INTERNAL, IKE

G. Lohnert
M. Bürger
W. Scheuermann

Synthesis on Requirements for Improvement of Nuclear Data

Deliverable

W. Bernnat
M. Mattes
J. Keinert

Stuttgart, 20 October 2004

Under the contract of the European Union (5th Framework Program) no. FIKI-CT-2000-00020.

rev. no	date	description
B	20.10.2004	Final issue
A	15.03.2003	First issue

author : M. Mattes	reviewed : W. Bernnat
1	Approved:
HTR-N-02-05-D-2.2.2	

Table of contents

List of figures

Introduction

1. Cross section libraries

The neutronics calculations for HTR's should be based on reliable and validated cross section evaluations. At beginning of the project the evaluations JEF-2.2, JENDL-3.2 and ENDF/B-VI until version VI.5 were available. At the beginning of 2004 also newer evaluations or new releases of single cross section data sets were published, especially JEFF-3.0, JENDL-3.3 and ENDF/B-VI up to release 8 /1,2,3,4,5/ and even preliminary data for ENDF/B-VII.

For the neutronics calculations both continuous data e. g. for the Monte Carlo code MCNP /6/ or comparable codes and multigroup data sets were processed or updated mainly based on the evaluations JEF-2.2, ENDF/B-VI and JENDL-3.2. The processing code for these data is mainly the program system NJOY /7/.

Most of the calculations in WP1, WP2 and WP3 were based on these evaluations. Some care has to be taken when U-235 and U-238 is used from ENDF/B-VI.5 or cross sections for Th-233, Pa-233 and U-233 as well as Eu fission products from JEF-2.2. Meanwhile improved data sets are available from JEFF-3, JENDL-3.3 and ENDF/B-VI.8 and ENDF/B-VII in future. Further work, new measurements and new evaluations will be made e. g. at LANL for some Am, Np Isotopes in the frame of the Advanced Fuel Cycle Initiative (AFCI).

For the moderator graphite several data sets were generated based on comparable old (but widely used) scattering laws and newer data sets based on scattering laws derived from ENDF/B and an alternative frequency distributions (see Difilippo et.al, and Awari et. al) /8,9/.

2. Multigroup libraries

The multigroup libraries which can be used for deterministic transport calculations and multigroup Monte Carlo are based mainly on JEF-2.2 and ENDF/B-VI. The structure of the libraries is ordered according to the AMPX library of the SCALE /10/ system. A list is given in **table 5**. Since the ENDF-6 format does not use resonance parameters in the AMPX compatible form, no resonance parameter are stored on the AMPX library. The resonance shielding is performed by solving the slowing down equation for the energy range of 1eV- 2keV for a hyperfine energy grid with up to 26,000 points using a first collision probability method for 1D cells /11/. Overlapping resonances can be taken into account by this method for all nuclides in the fuel, structure material or moderator. The library contains practically the same nuclides as the corresponding MCNP library with the exception of fission products for which - with few exceptions - not the full scattering matrix is stored but only the capture and scattering cross section.

The generated data were tested extensively against experiments and benchmarks /12,13,14/. Details of these benchmarks calculations are given in /15/.

3. Covariance data

- There are strong differences in covariance data of different data sources which lead to differences in uncertainty estimation:
  - uranium fuel U-235 fission 0.21 % (JEF-2.2), 0.08 %(IRDF90)
  - uranium fuel U-238 total 0.47% (JEF-2.2 incomplete), 0.26% (IRDF90)
  - plutonium fuel: also strong differences between JEF-2.2 and IRDF90
- The covariance data for uncertainty analysis are not complete in the different data evaluations; there are few applications for thermal reactors.
- Covariance data for actinides are in IRDF90, JEF-2.2 (JEFF-3.0) ENDF/B-VI.7 and CENDL-2.1.

For a number of actinides covariance data are plotted in fig. 1 to 17.

4. Literature

1. The JEF-2.2 Nuclear Data Library, JEF-Report 17 , April 2000.

2. ENDF/B-VI Summary Documentation", BNL-NCS-17541 (ENDF-201), 4th edition, (Oct. 1991)

3. Nakagawa, K.Shibata, S.Chiba, T.Fukahori, Y.Nakajima, Y.Kikuchi, T.Kawano, Y.Kanda, T.Ohsawa, H.Matsunobu, M.Kawai, A.Zukeran, T.Watanabe, S.Igarasi, K.Kosako, T.Asami: "Japanese Evaluated Nuclear Data Library Version 3 Revision-2: JENDL-3.2", J. Nucl. Sci. Technol., 32, 1259 (1995).

4. C. Nordborg, M. Salvatores, "Status of the JEF Evaluated Data Library", Proc. Int. Conf. on Nuclear Data for Science and Technology, Gatlinburg 1994, p.680 . JEFF-3.0 Starter File (JEF/DOC 1999)

5. H. Takano: Validation of JENDL-3.3 by Criticality Benchmark Testing. Int. Conf. on Nuclear Data for Science and Technology, Tsukuba, Japan, 7-12th Oct 2001

6. J. F. Briesmeister, Editor, "MCNP -- A General Monte Carlo N-Particle Transport Code", Los Alamos National Laboratory report LA-12625-M (March, 1997)

7. R. E. MacFarlane, D. W. Muir, "The NJOY Nuclear Data Processing System – Version 91", LA-12740-M (1994)

8. Difilippo,F.C.; Renier,J.P.; Hawari, A.I.: Benchmarks for the Scattering Kermel of Graphite. Proceeding of the PHYSOR 2002: International Conference on the New

9. Mac Farlane,R.E. : New Thermal Neutron Scattering Files for ENDF/B-VI Release 2. LA-12639-MS (ENDF-356) (1994)

10. W. Bernnat, D. Lutz, J. Keinert, M. Mattes, "Erstellung und Validierung von Wirkungsquerschnittsbibliotheken im SCALE-Format auf der Basis der evaluierten Dateien JEF-2 und ENDF/B-VI für Kritikalitäts- und Reaktorauslegungsberechnungen sowie Störfallanalysen", IKE 6-189 (1994)

11. D. Emendörfer, K.H. Höcker: Theorie der Kernreaktoren Vol. I: Der Stationäre Reaktor, BI ISBN 3-411-01599-3 (1982)

12. Bernnat, W., et al.: Application of Nuclear Data Libraries Based on JEF-2.2, ENDF/B-VI and JENDL-3.2 to LWR Criticality and Burnup Problems. Int. Conf. on Nuclear Data for Science and Technology, Triest 1997

13. Bernnat, W., M. Mattes, S. Langenbuch, F. Moser, W. Zwermann: Analysis of LWR Benchmarks based on different Methods and Nuclear Data Evaluations, Int. Conf. PHYSOR 2000, Pittsburgh, Pennsylviania, USA, May 2000, p. 3402

14. Bernnat, W., S. Langenbuch, M. Mattes, W. Zwermann: Validation of Nuclear Data libraries for Reactor Safety and Design Calculations. Proc. Int. Conf. Of Nuclear Data for Science and Technology ND2001, Tsukuba, Japan, Vol. 1 ISSN 0022-3131 p. 884 (2001)

15. HTR-N-05-D-2.1.5, Validation of cross section libraries for analysis of thermal reactors

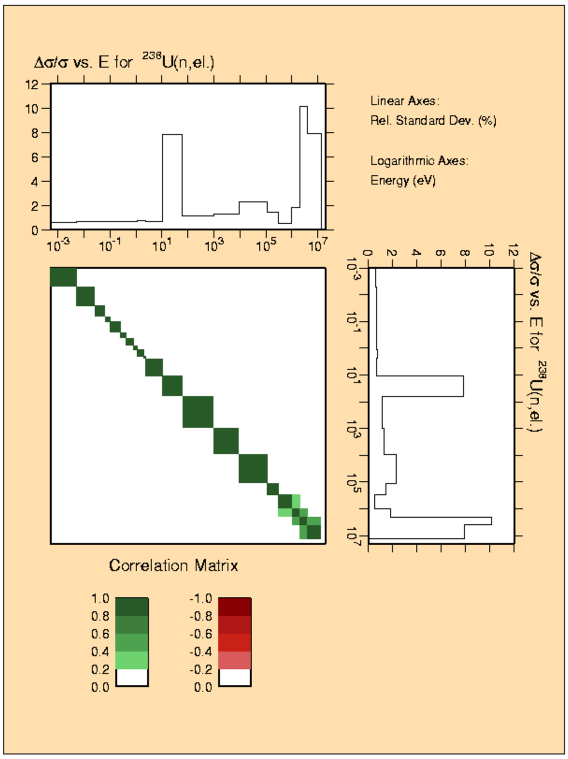

Fig. 1: correlation matrix for ^{238} U-reaction (n, el.)

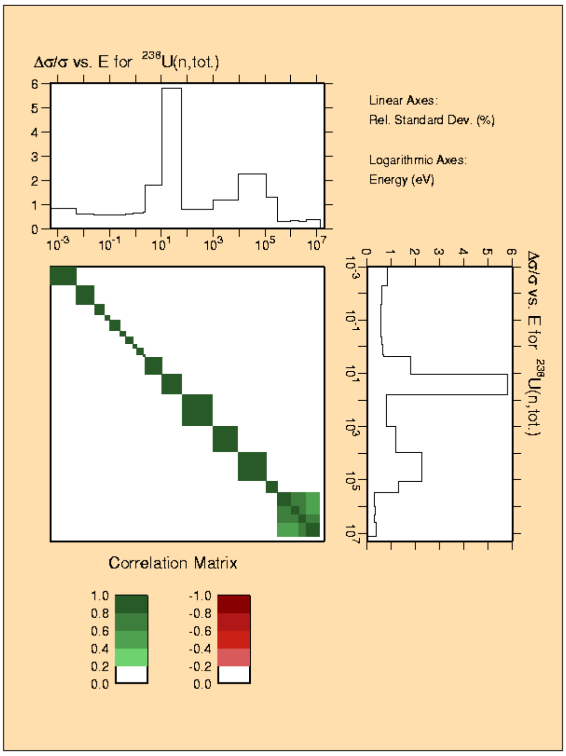

Fig. 2: correlation matrix for ^{238} U-reaction (n, tot)

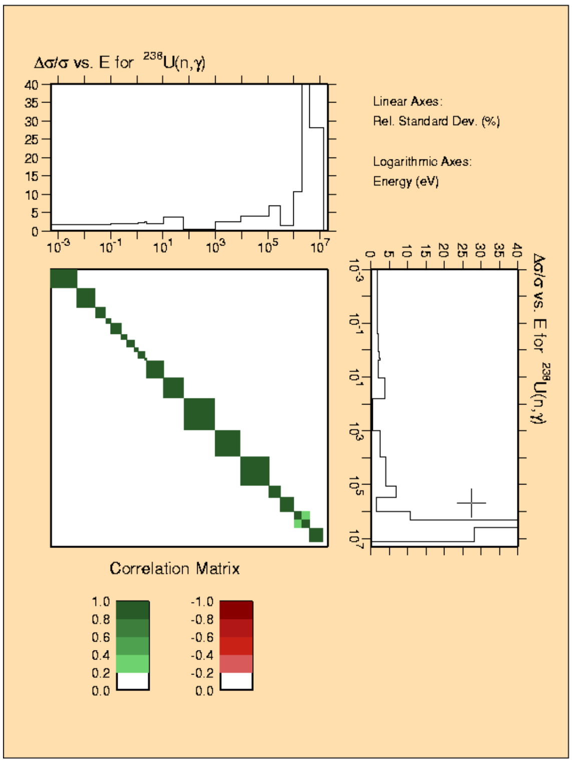

Fig. 3: correlation matrix for ^{238} U-reaction (n, γ)

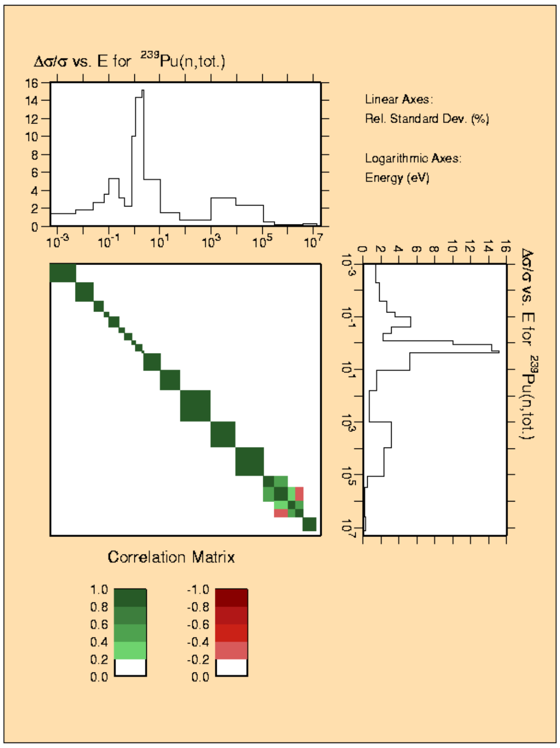

Fig. 4: correlation matrix for ^{239} Pu-reaction (n, tot)

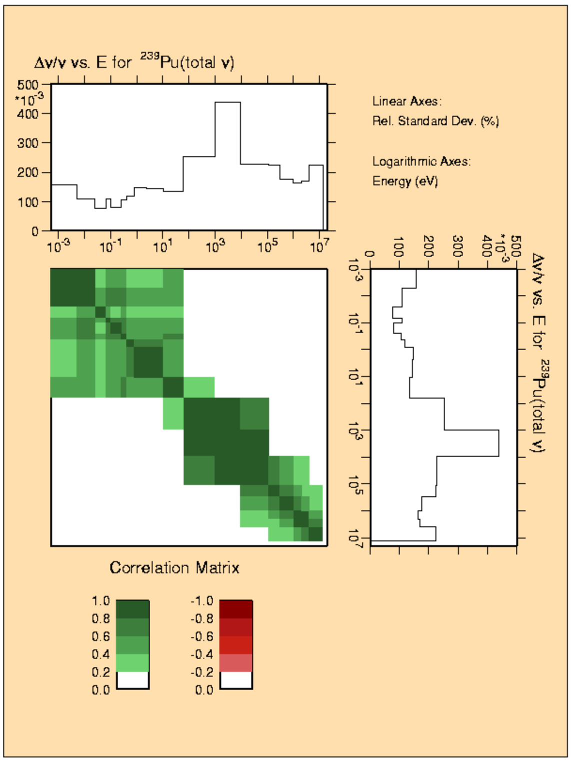

Fig. 5: correlation matrix for ^{239}Pu (total ν)

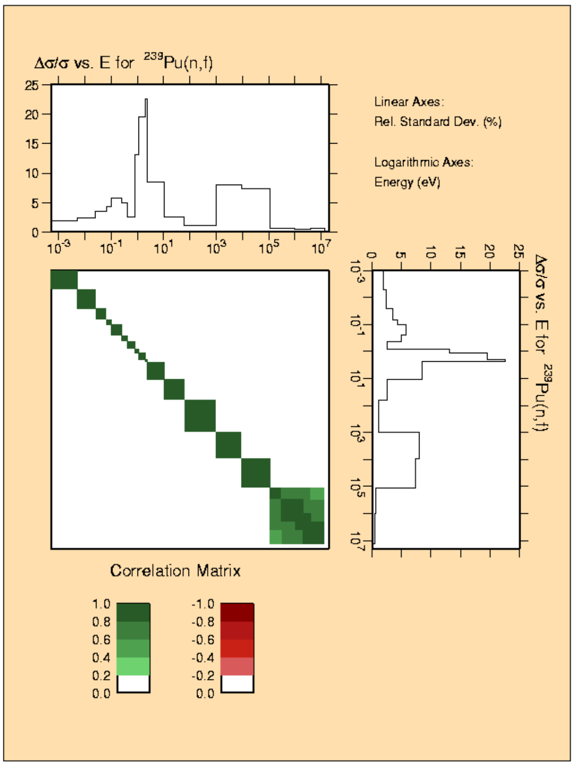

Fig. 6: correlation matrix for ^{239}Pu-reaction (n, f)

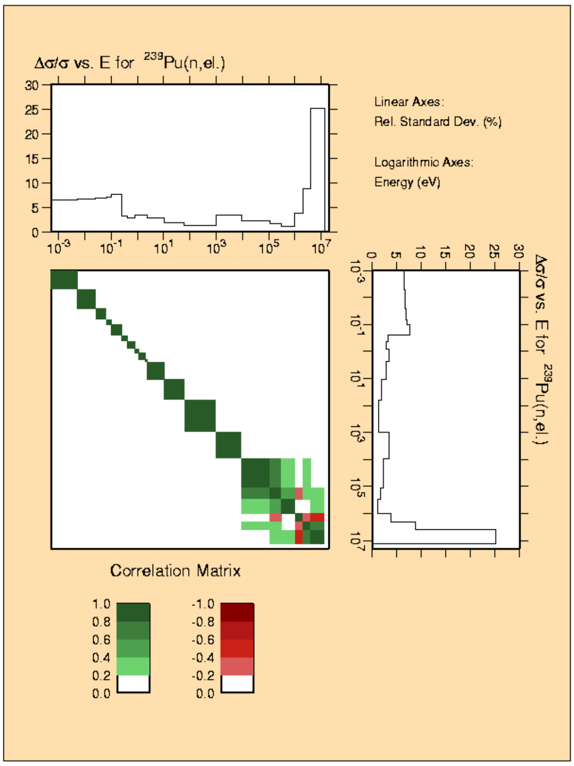

Fig. 7: correlation matrix for ^{239}Pu-reaction (n, el.)

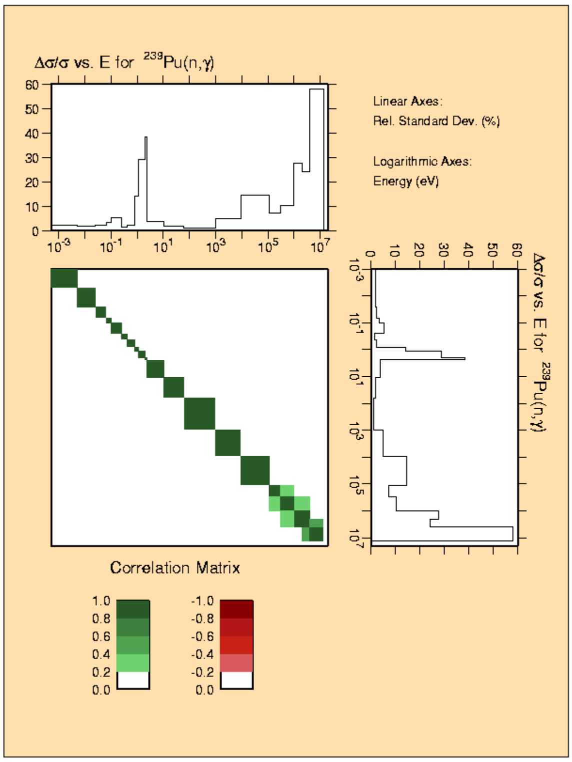

Fig. 8: correlation matrix for ^{239}Pu-reaction (n, γ)

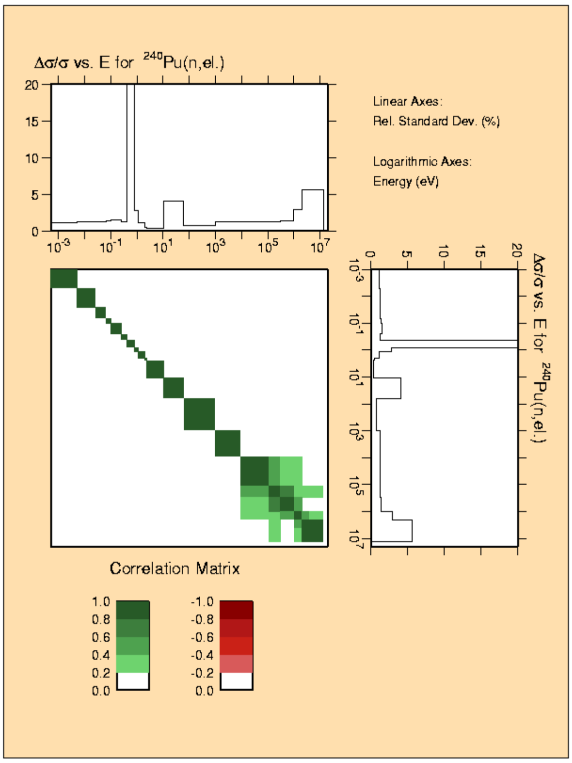

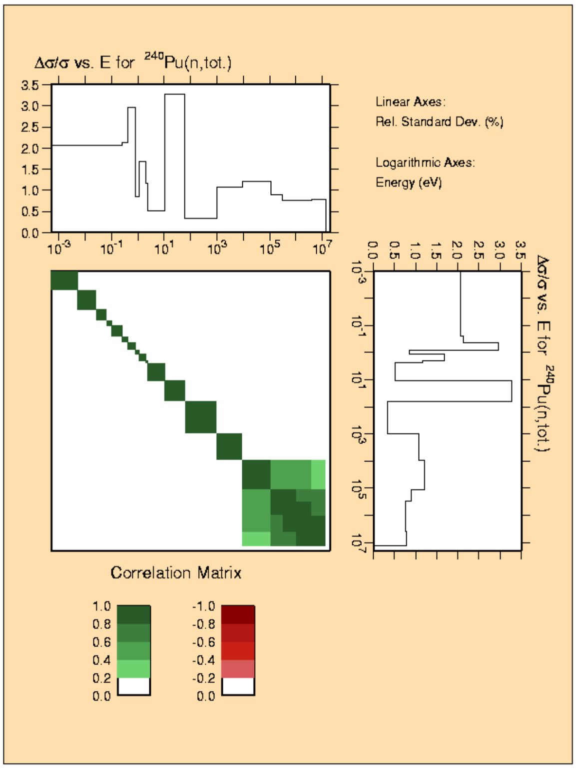

Fig. 9: correlation matrix for ^{240} Pu-reaction (n,el.) Fig. 10: correlation matrix for ^{240} Pu-reaction (n, tot)

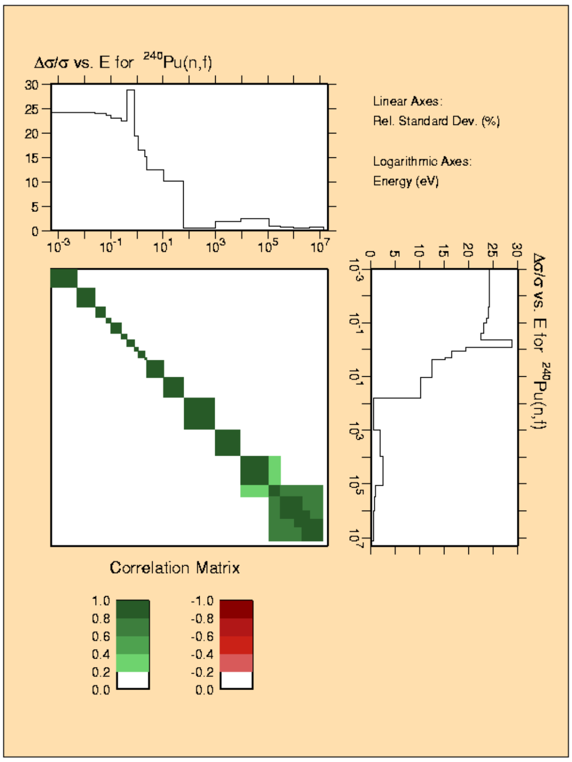

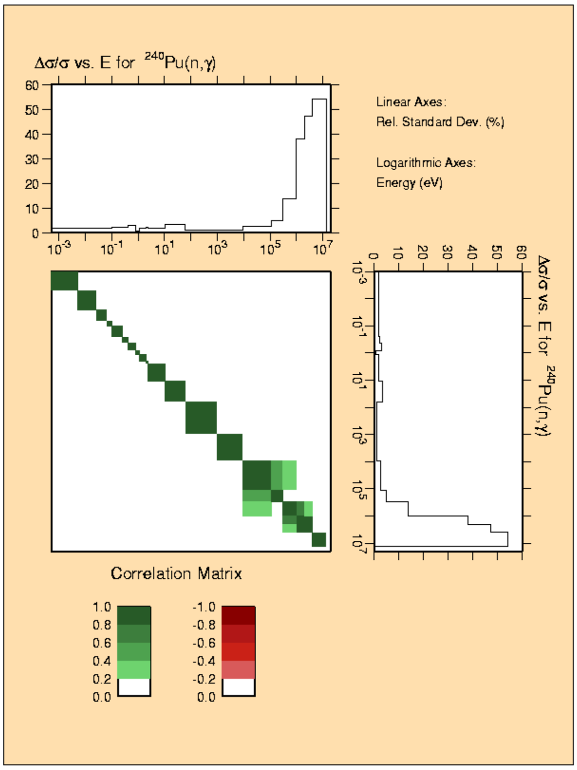

Fig. 11: correlation matrix for ^{240} Pu-reaction (n, f) Fig. 12: correlation matrix for ^{240} Pu-reaction (n, γ)

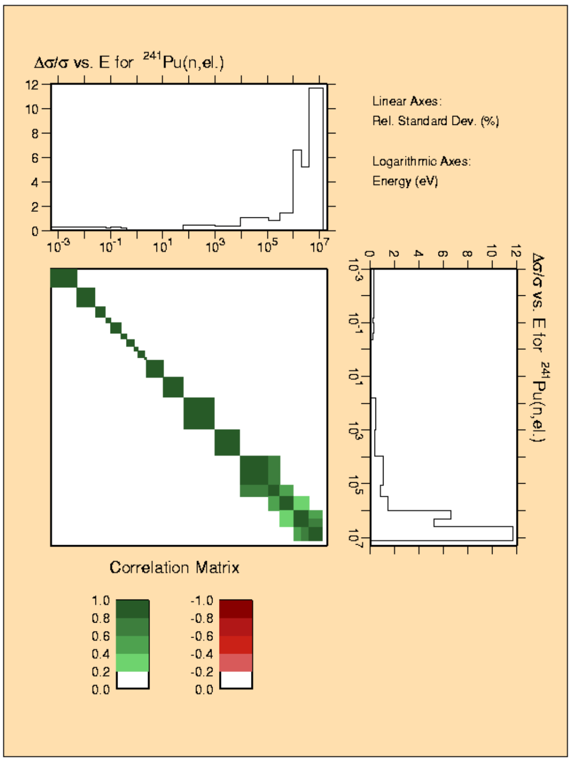

Fig. 13: correlation matrix for ^{241}Pu-reaction (n, el.)

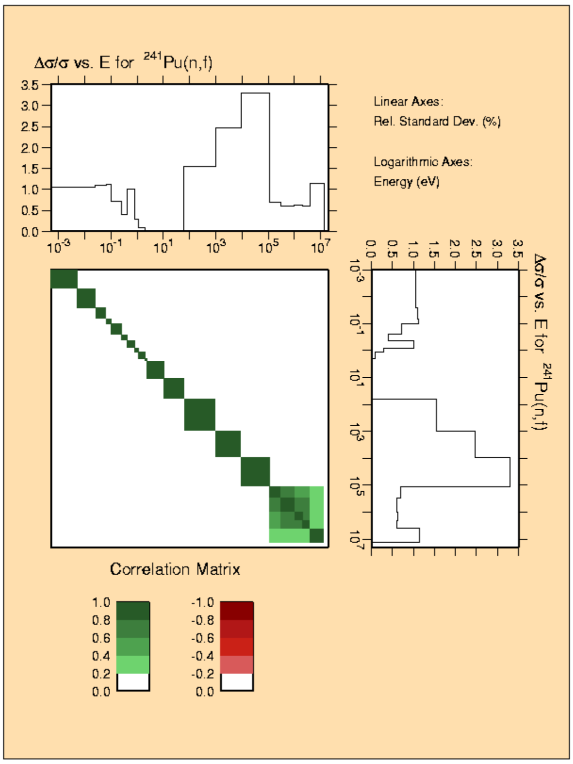

Fig. 14: correlation matrix for ^{241}Pu-reaction (n, f)

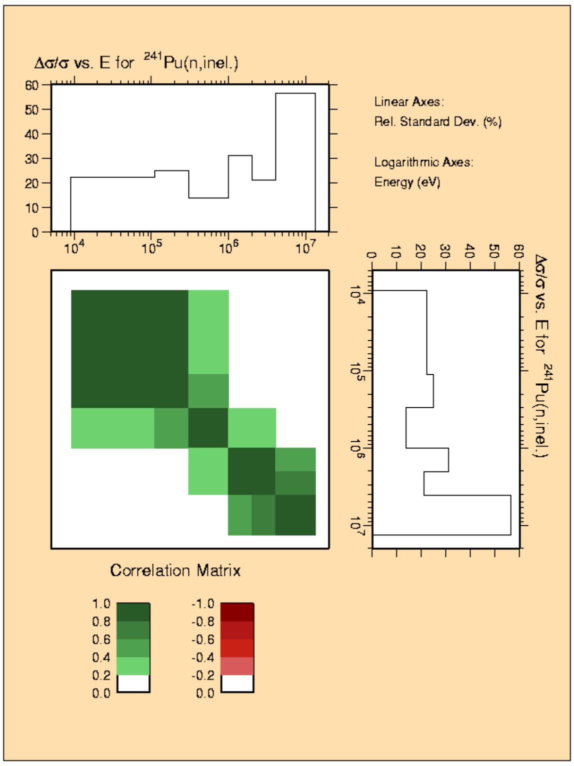

Fig. 15: correlation matrix for ^{241}Pu-reaction (n, inel.)

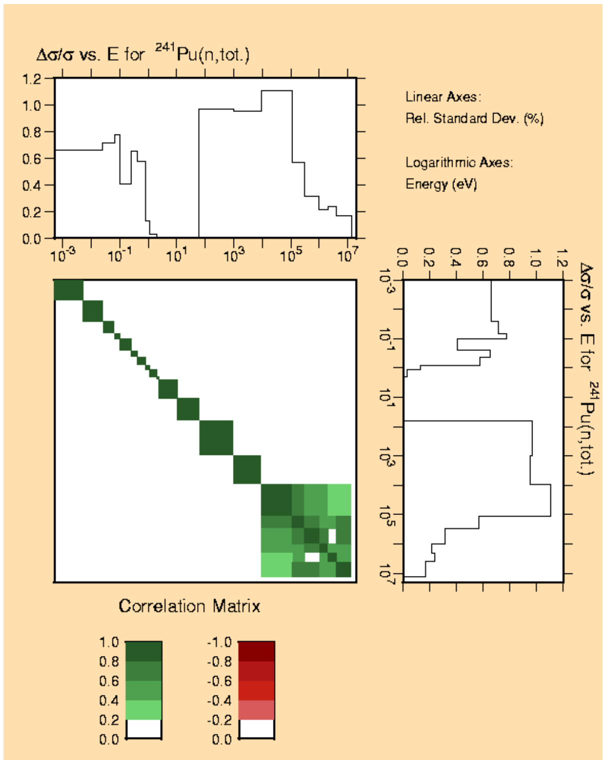

Fig. 16: correlation matrix for ^{241}Pu-reaction (n, tot)

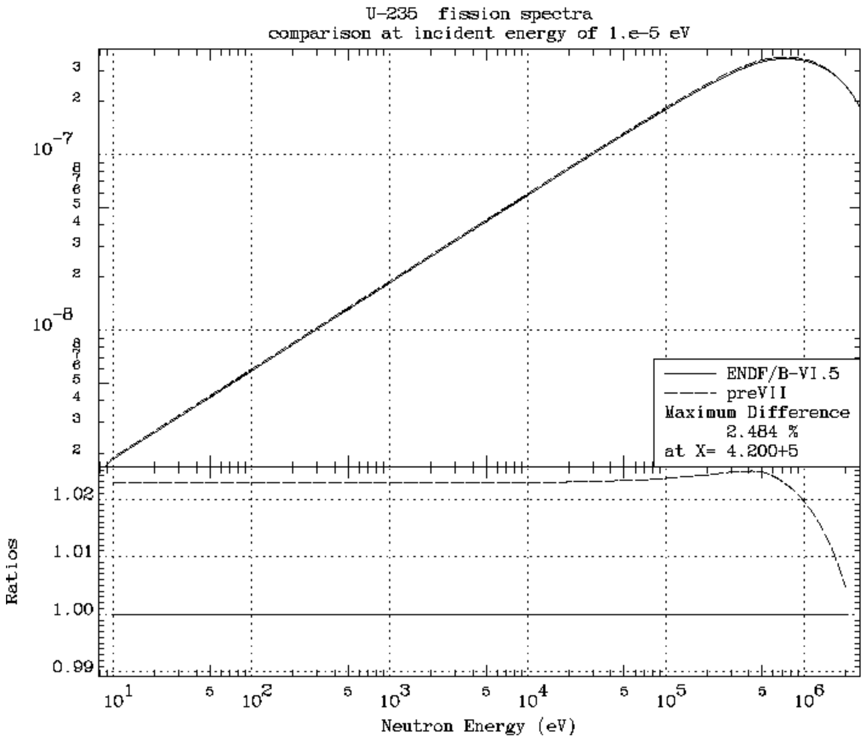

Fig. 17 New evaluations for U-235 fission spectra ENDF/B-VI vs. Pre ENDF/B-VII

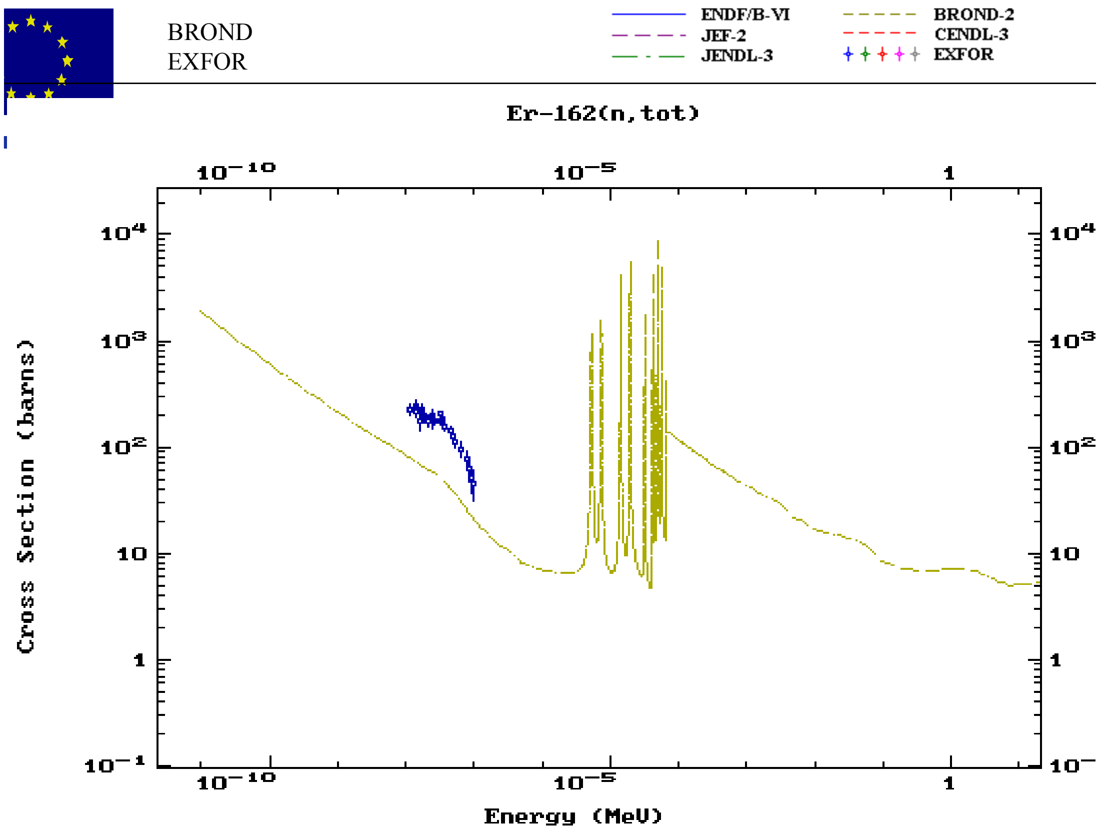

Fig. 18: Total cross section for Er-162

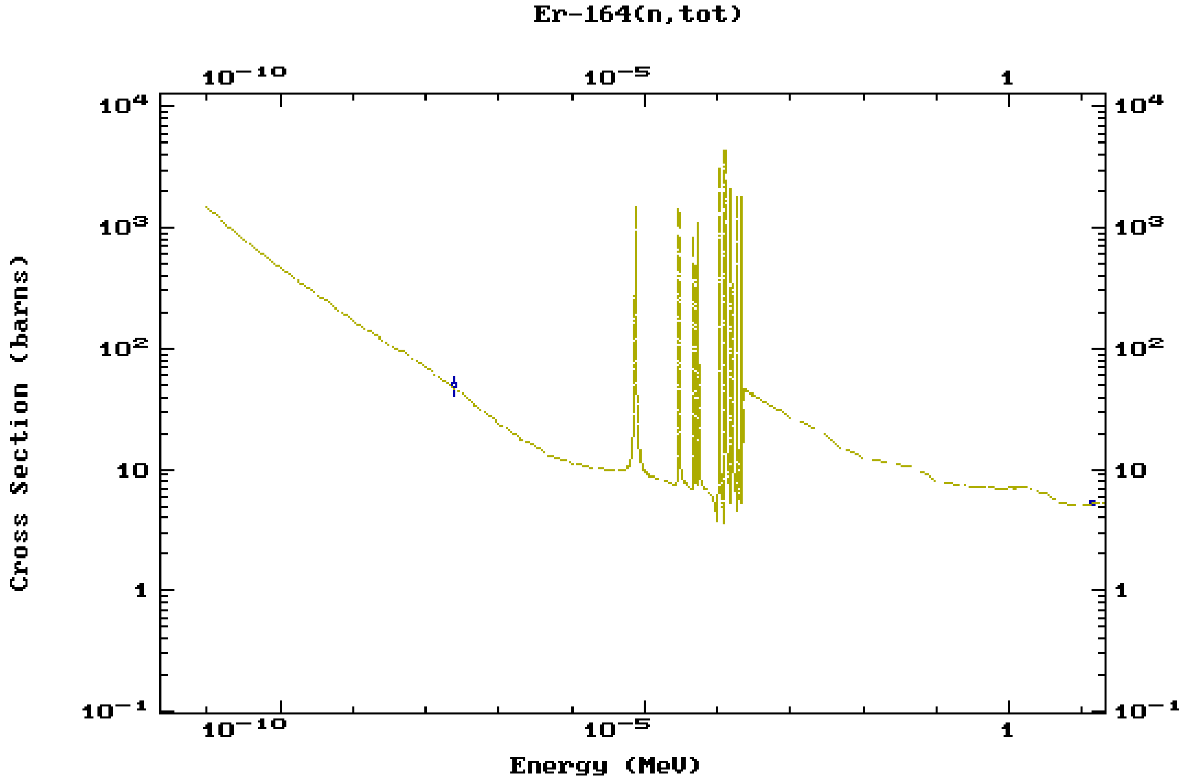

Fig. 19: Total cross section for Er-164

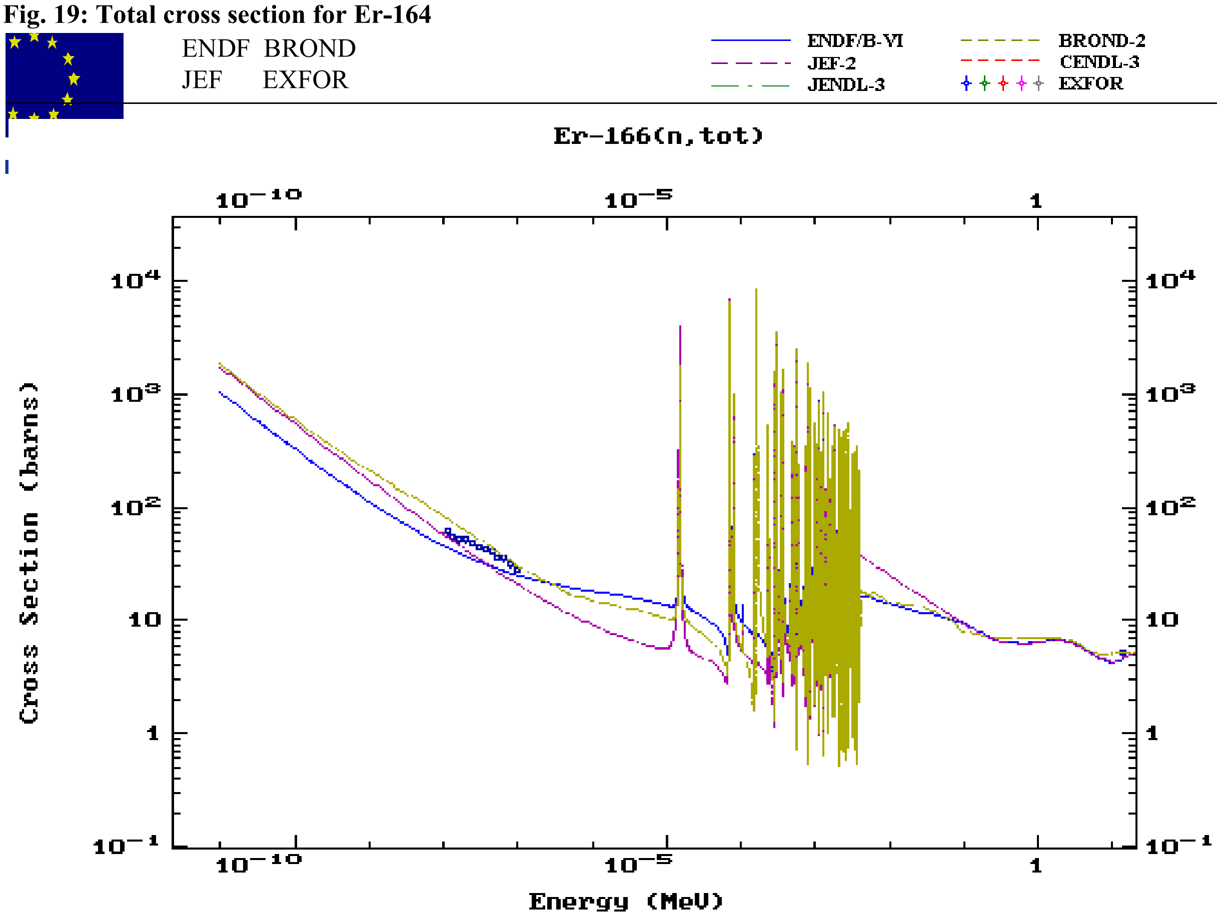

Fig. 20: Total cross section for Er-166

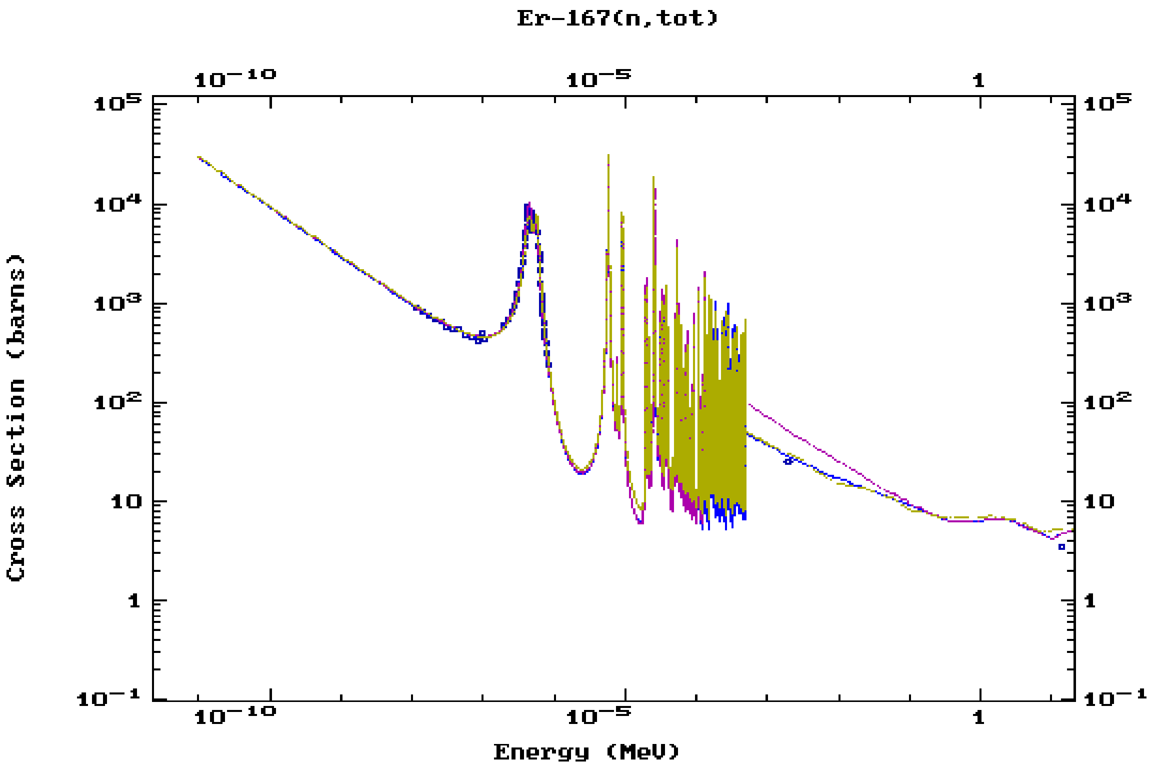

Fig. 21: Total cross section for Er-167

BROND
EXFOR

ENDF/B-VI
JEF-2
JENDL-3
BROND-2
CENDL-3
EXFOR

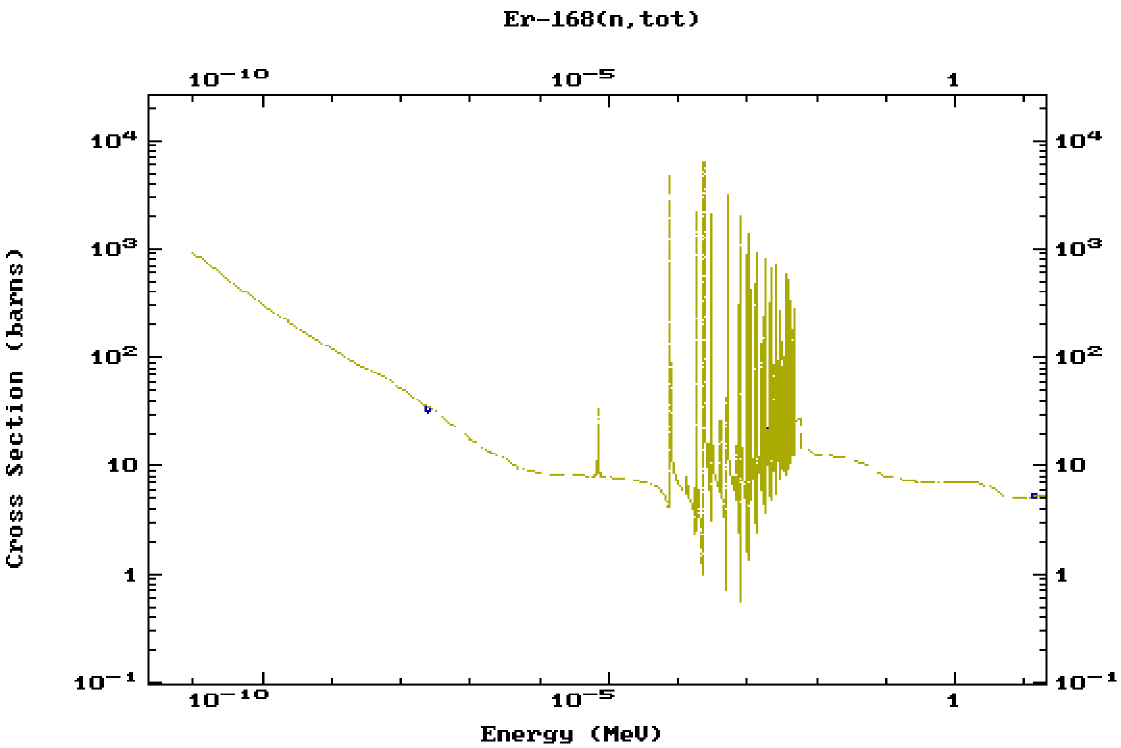

Fig. 22: Total cross section for Er-168

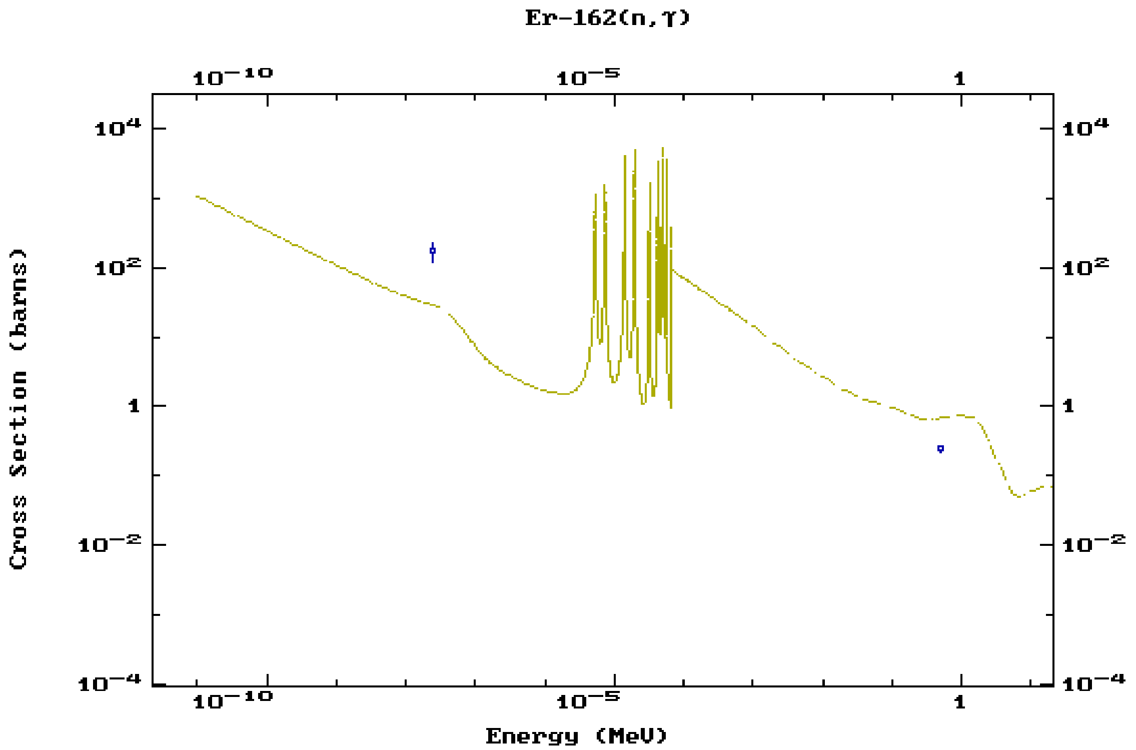

Fig. 23: N, gamma cross section for Er-162

BROND
EXFOR

ENDF/B-VI
JEF-2
JENDL-3
BROND-2
CENDL-3
EXFOR

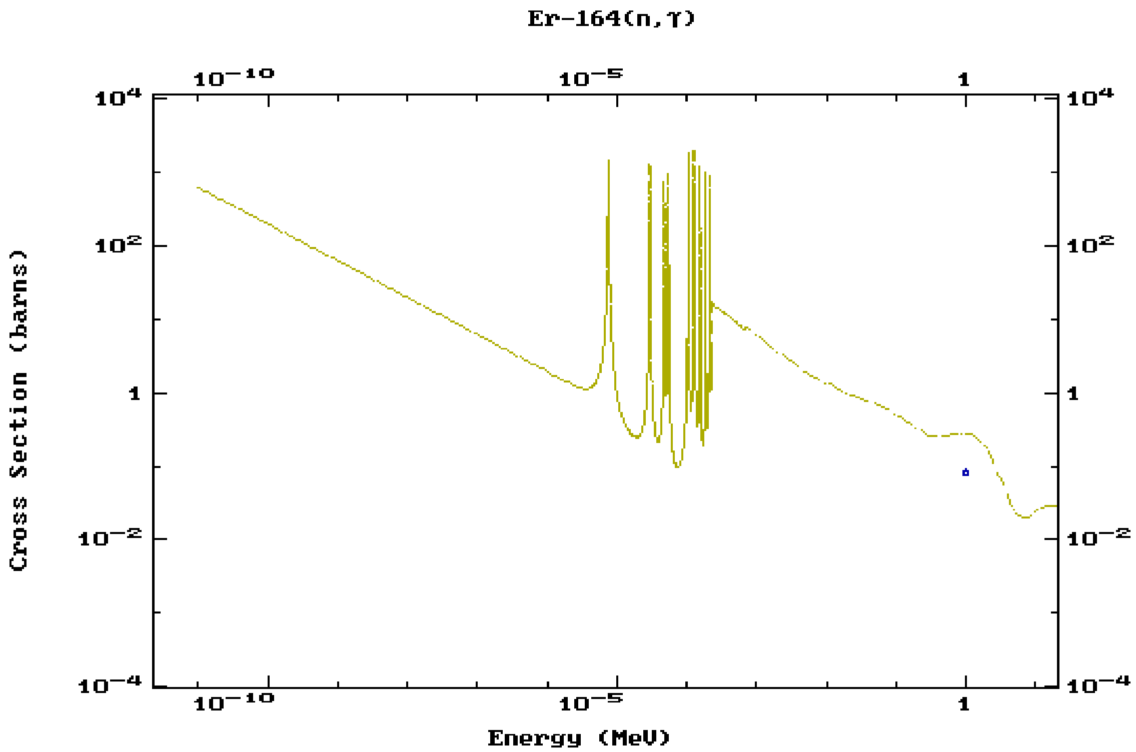

Fig. 24: N, gamma cross section for Er-164

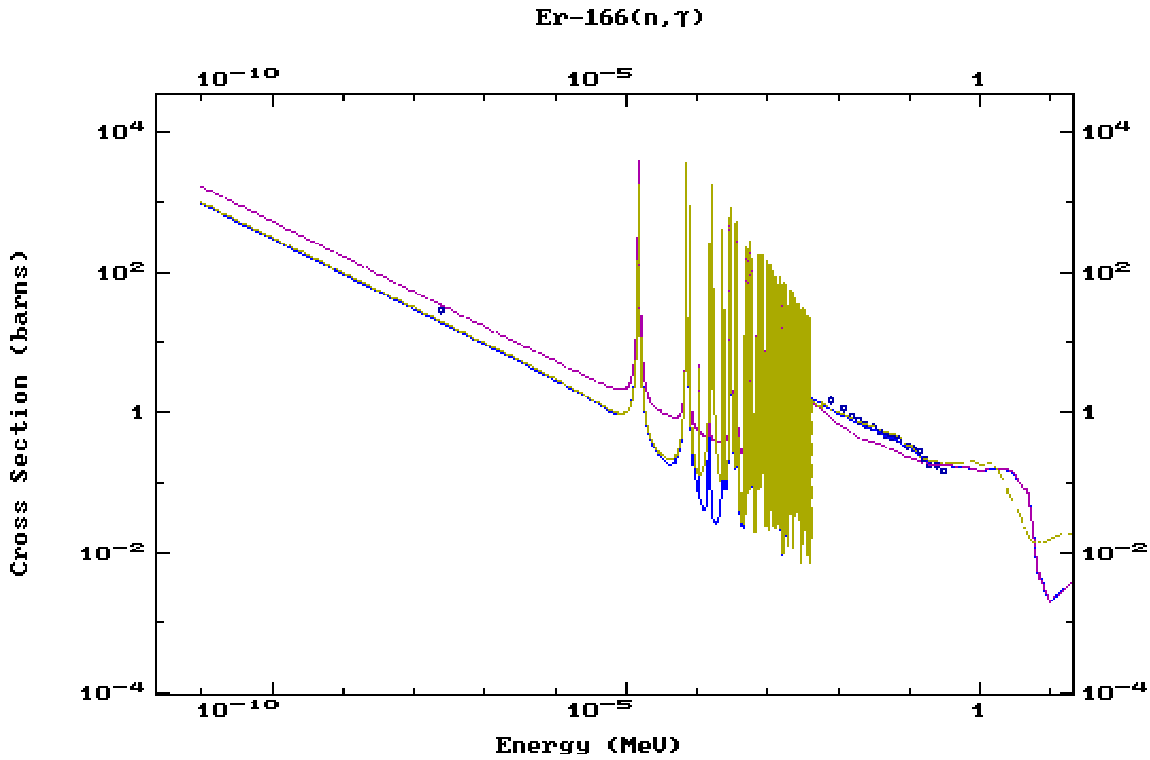

Fig. 25: N, gamma cross section for Er-166

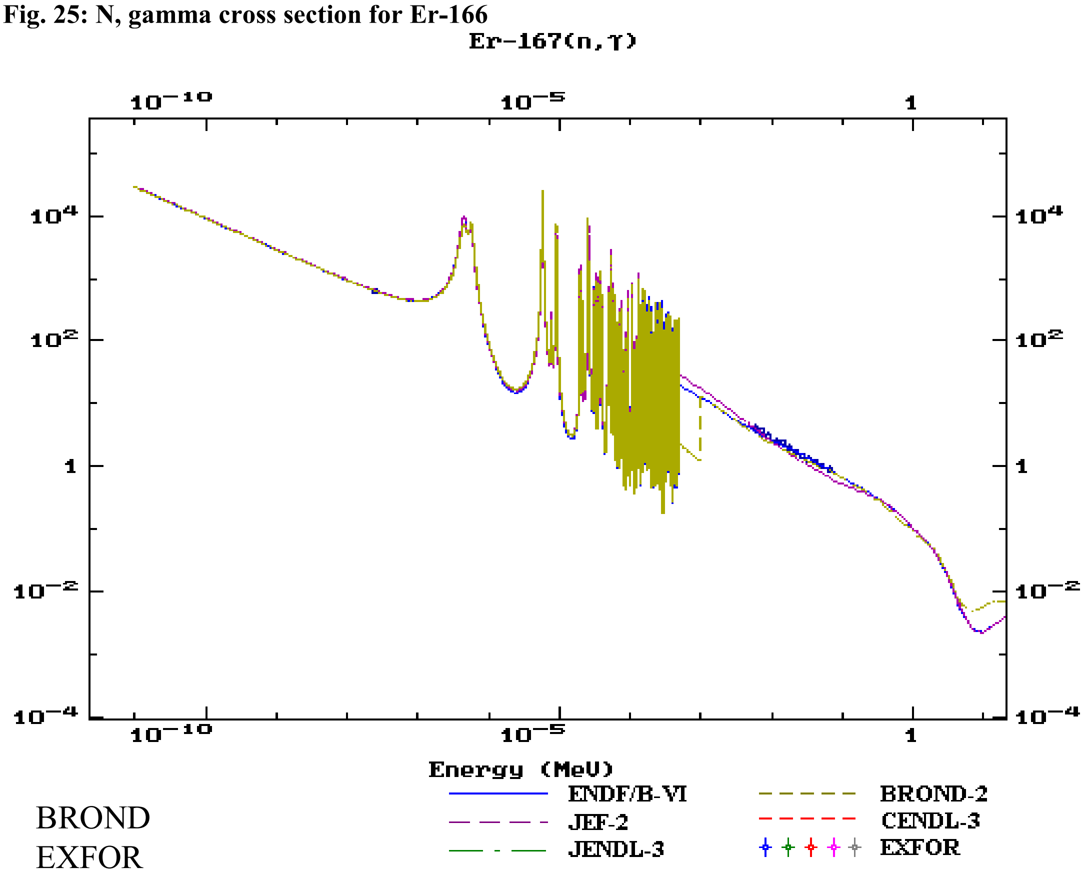

BROND
EXFOR

Fig. 26: N, gamma cross section for Er-167

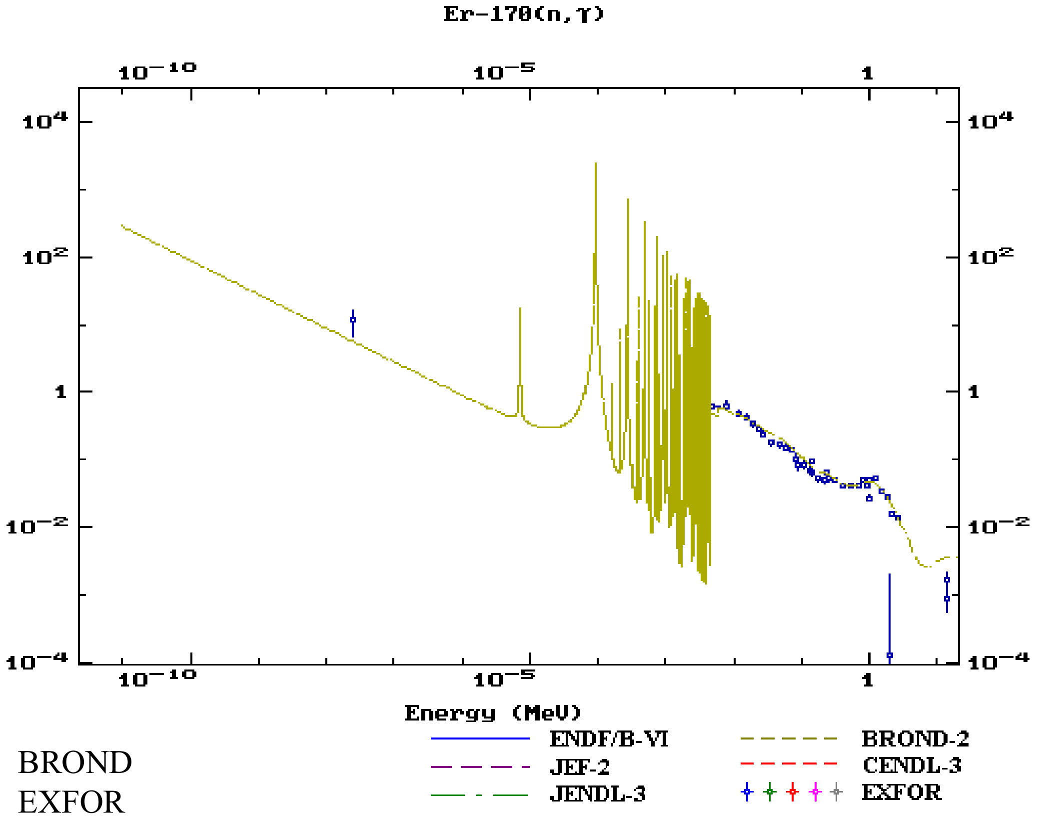

BROND
EXFOR

Fig. 27: N, gamma cross section for Er-170

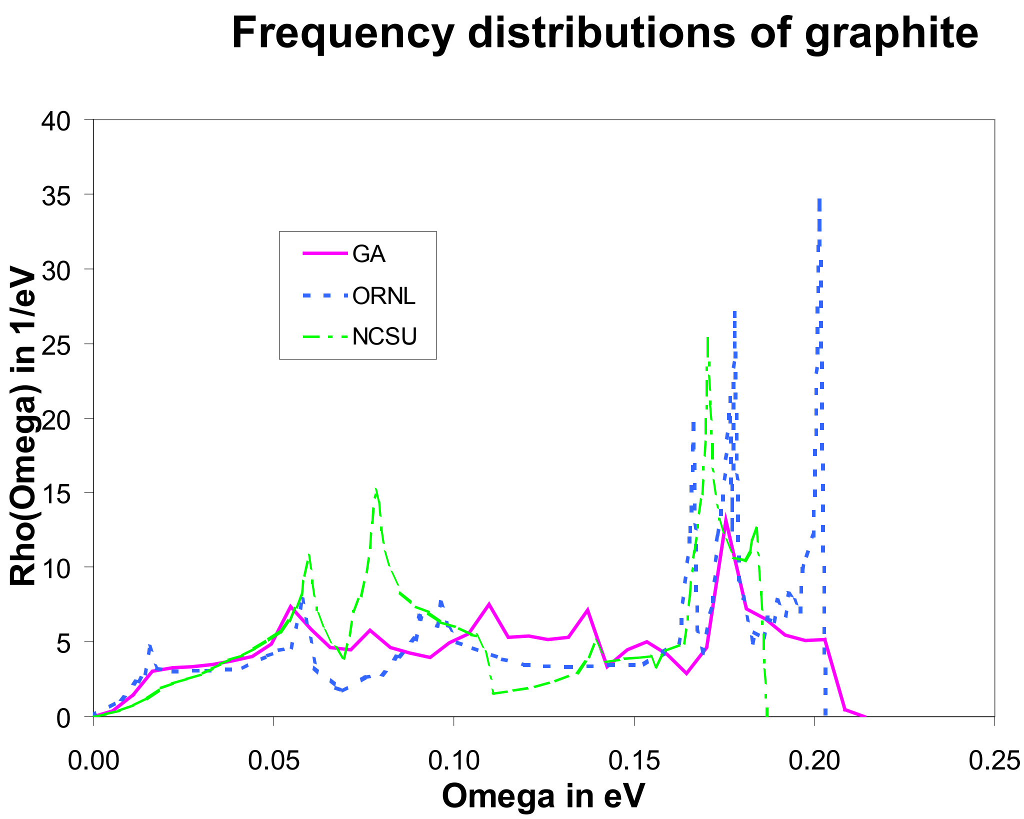

Fig. 28: Frequency distributions for graphite

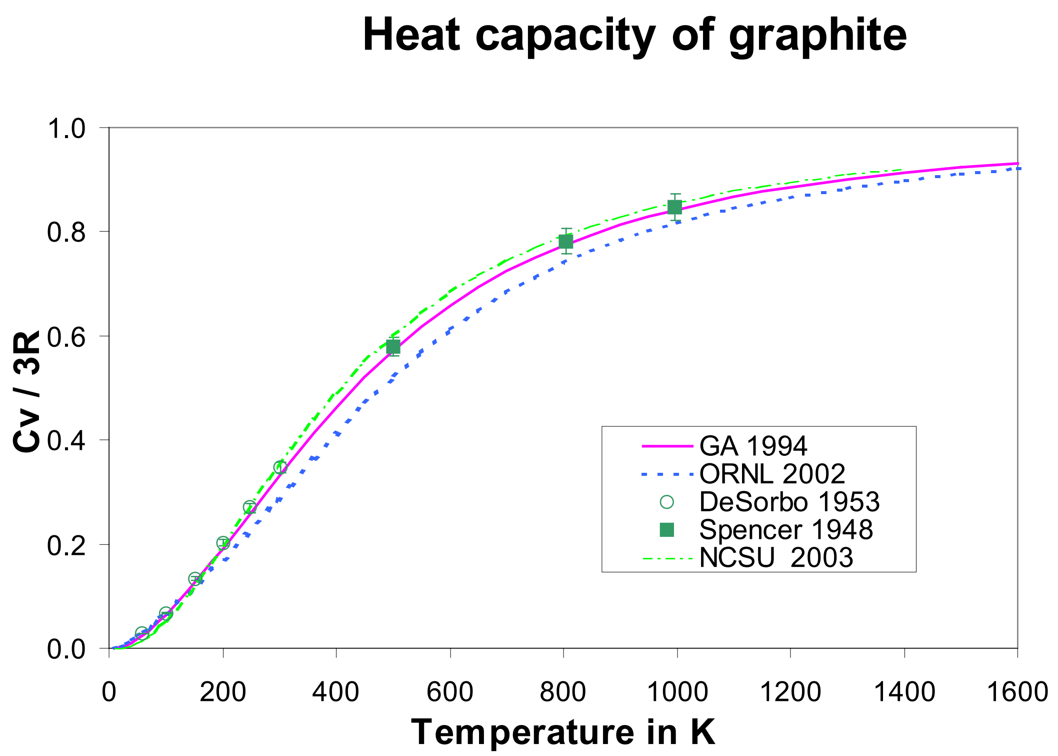

Fig. 29: Heat capacity of graphite

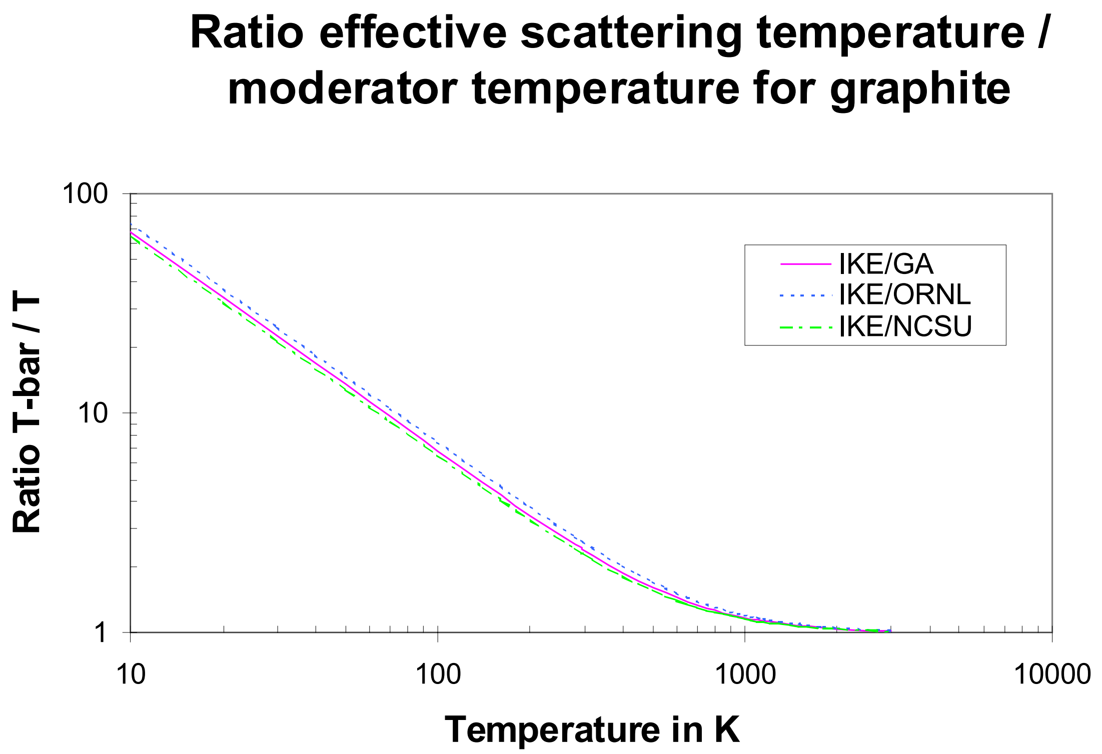

Fig. 30: Ratio of the effective scattering temperature and moderator temperature for graphite

Graphite Scattering Law data at room temperature (energy transfer 51.7 meV)

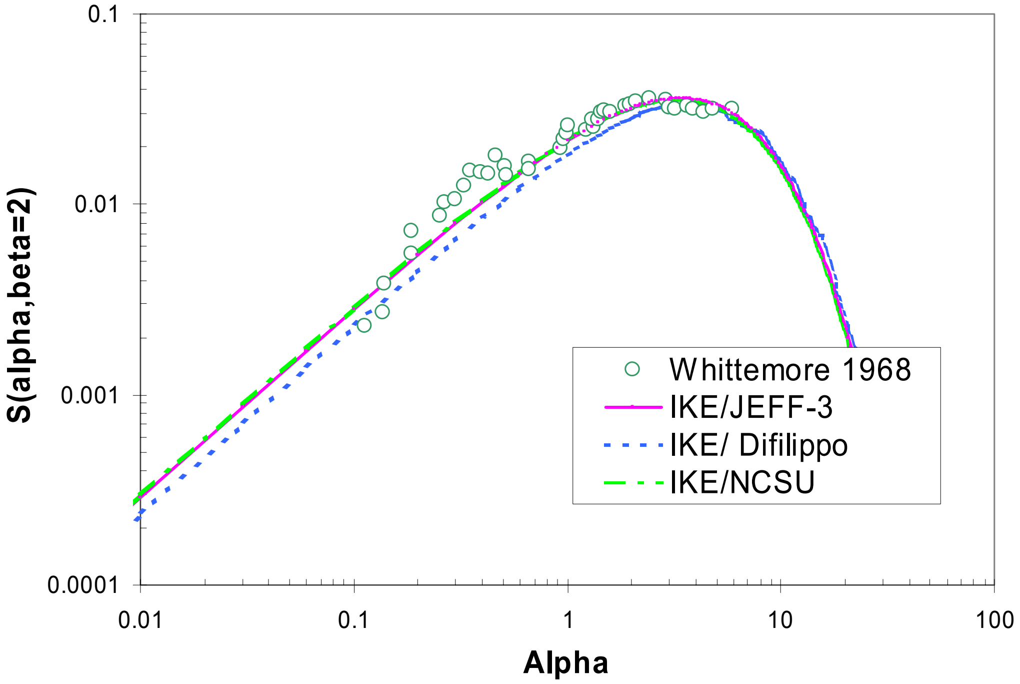

Fig. 31: Scattering law data at T=293 K for graphite (energy transfer 51.7 meV

Graphite Scattering Law data at room temperature (energy transfer 155.1 meV)

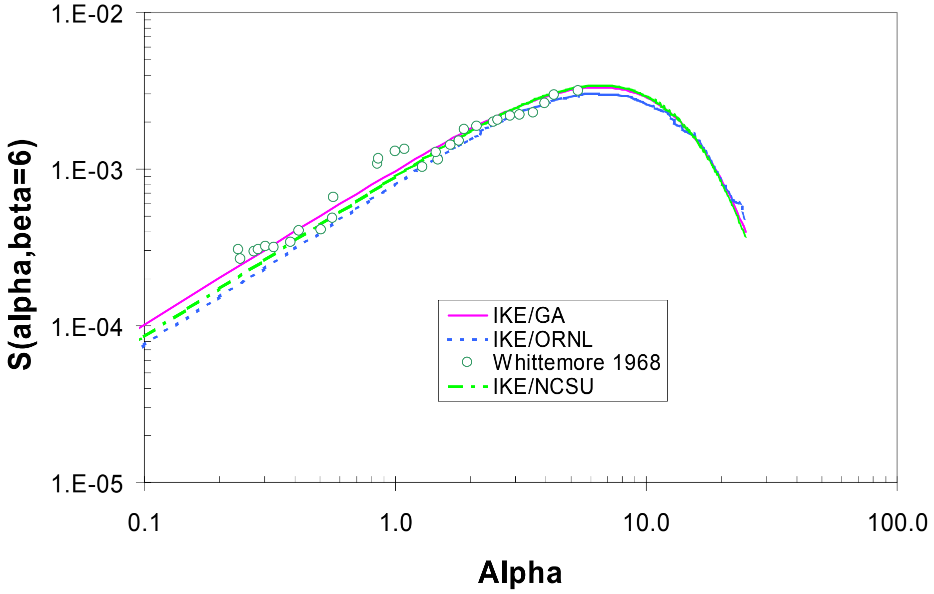

Fig. 32: Scattering law data at T=293 K for graphite (energy transfer 155.1 meV)

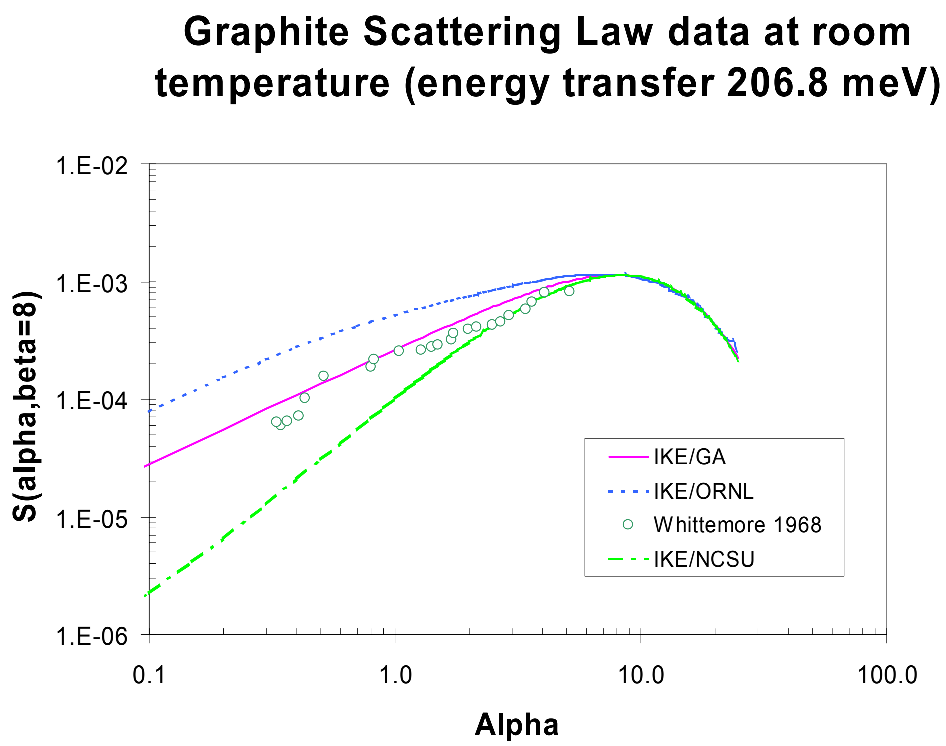

Fig. 33: Scattering law data at T=293 K for graphite (energy transfer 206 meV

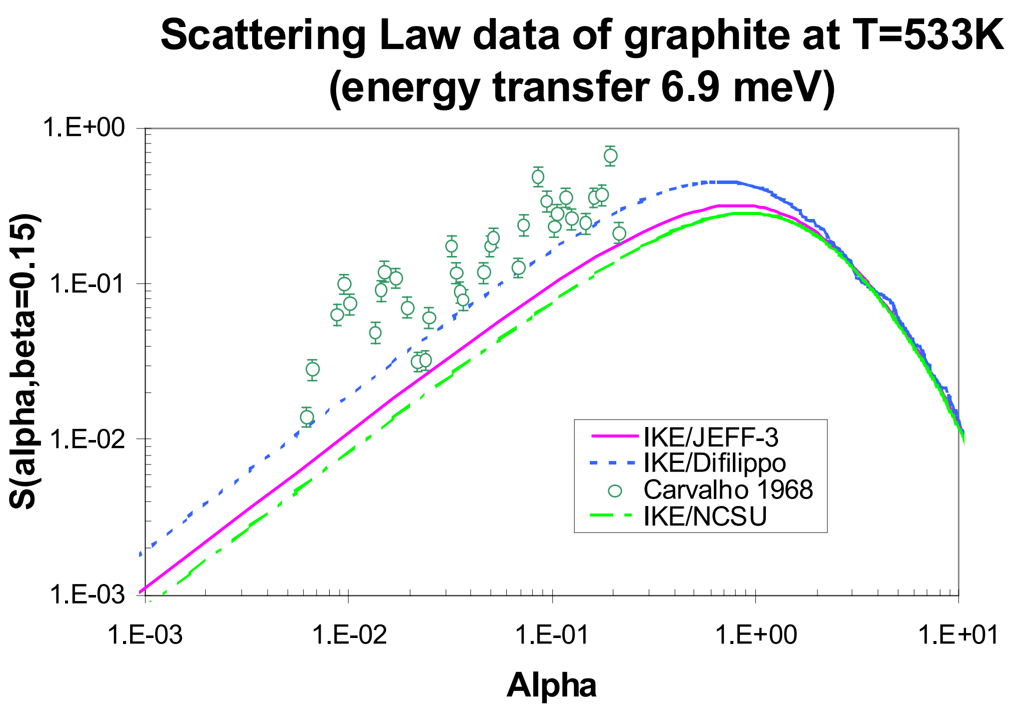

Fig. 34: Scattering law data at T=533 K for graphite (energy transfer 6.9 meV

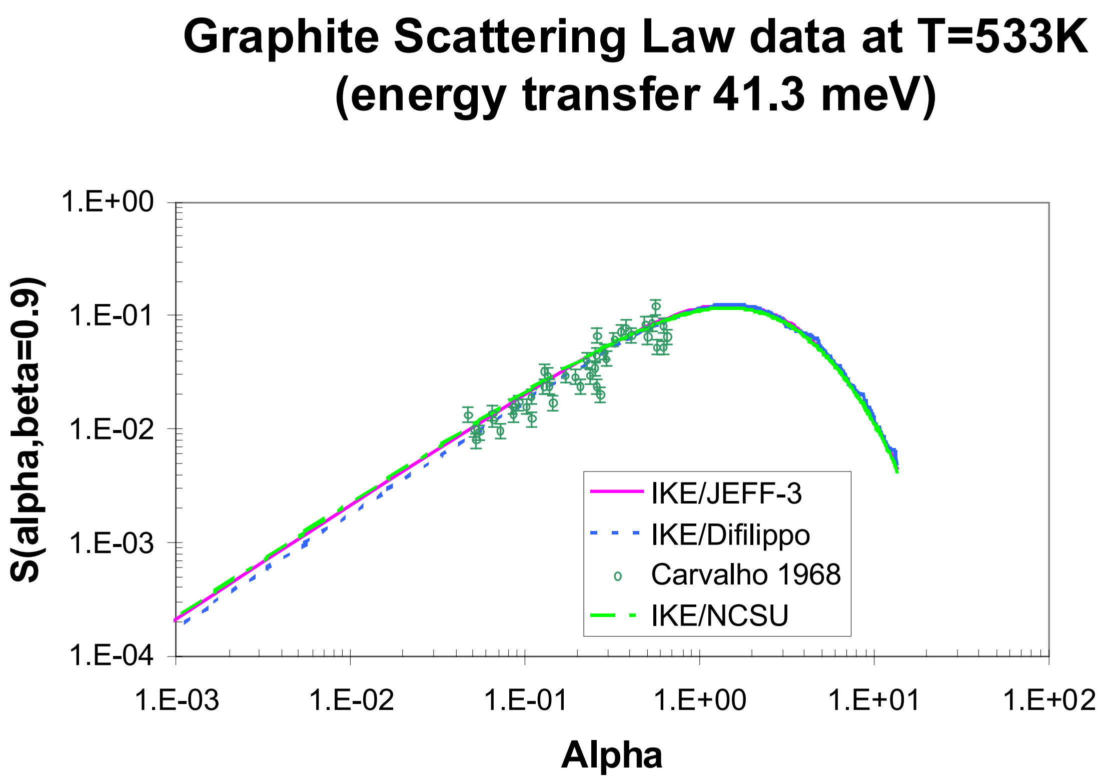

Fig. 35: Scattering law data at T=533 K for graphite (energy transfer 41.3 meV)

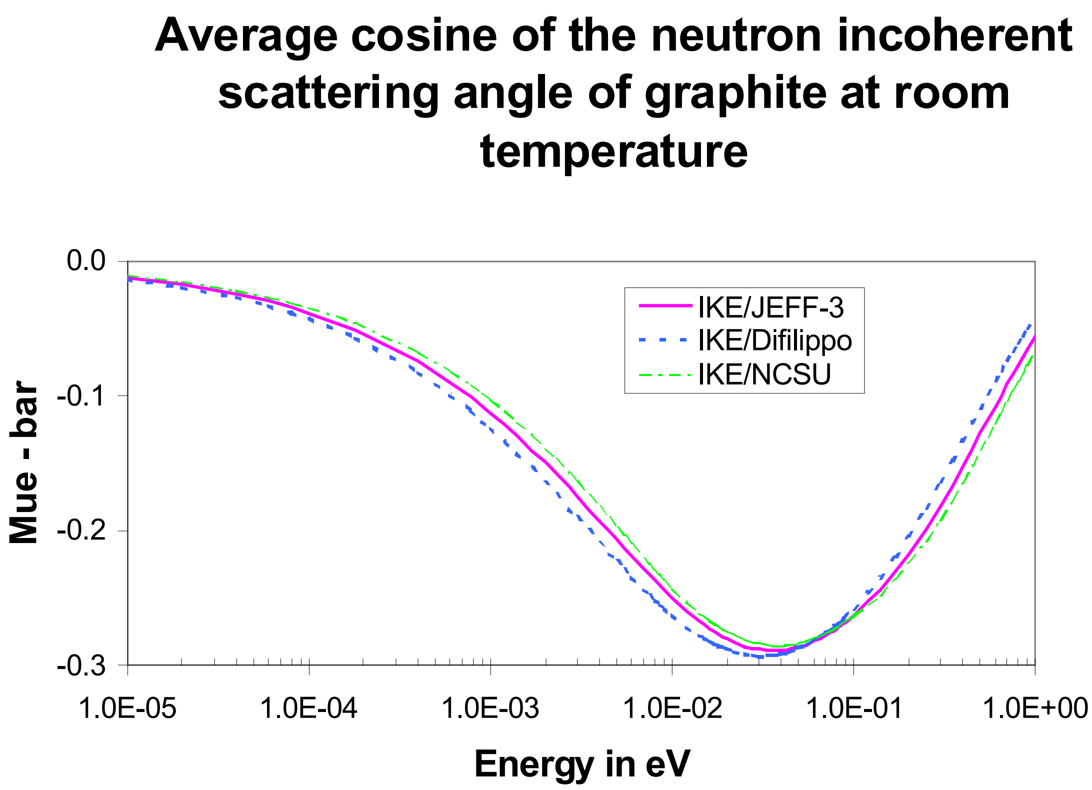

Fig. 36: Average cosine of the incoherent scattering angle of graphite at room temperature

Double differential neutron cross-section for graphite at room temperature (E0=0.325 eV, Theta=120 deg.)

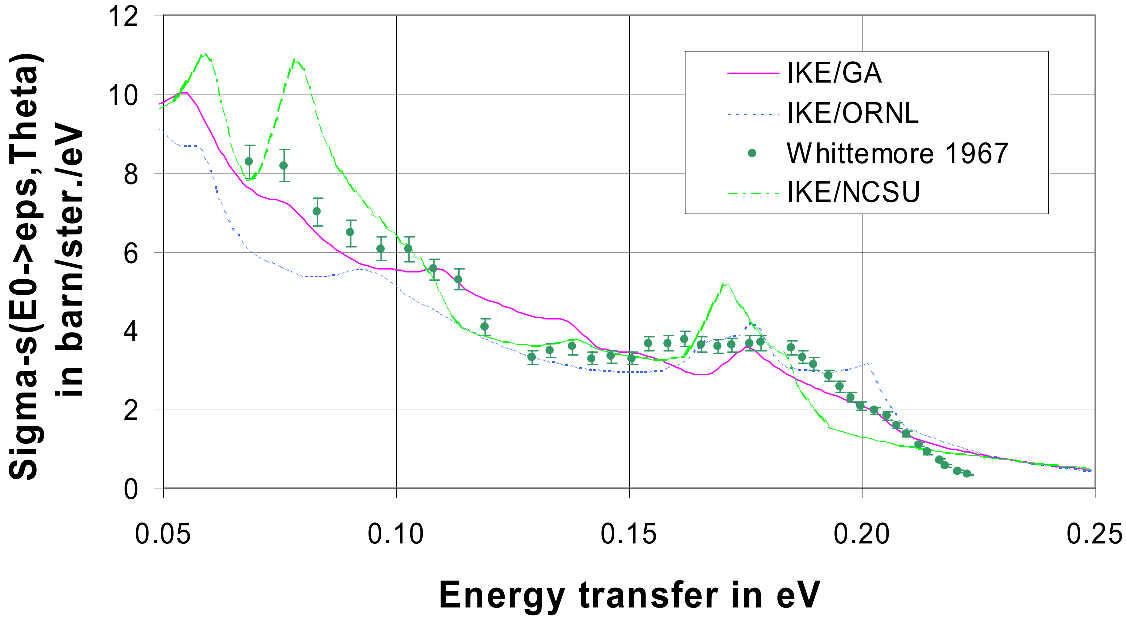

Fig. 37: Double different neutron scattering cross section for graphite at room temperature

Double differential neutron down-scattering cross-section for graphite at room temperature (E0=0.325 eV, Theta=120 deg.)

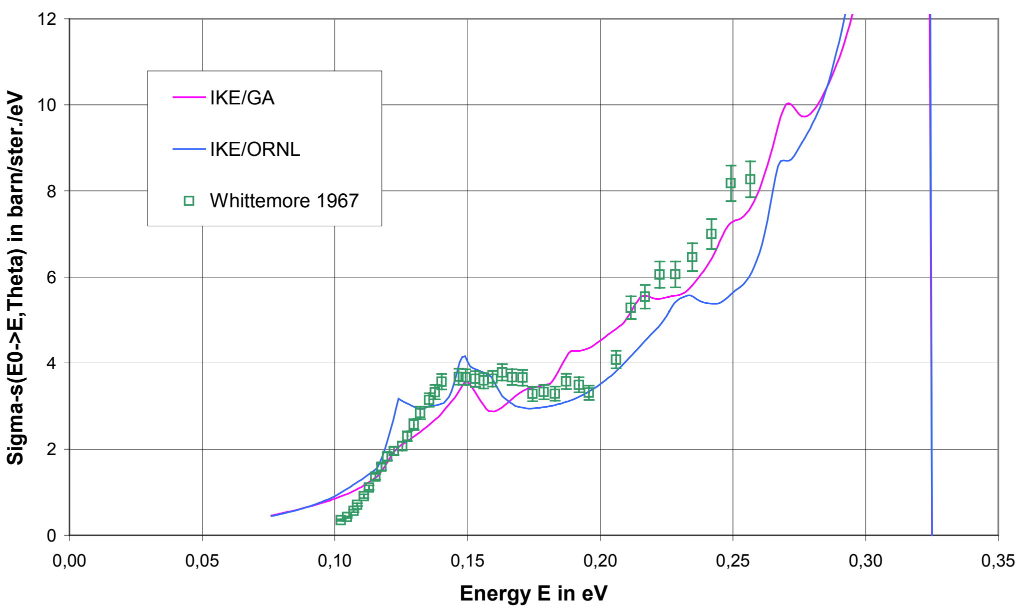

Fig. 38: Double different neutron downscattering cross section for graphite at room temperature

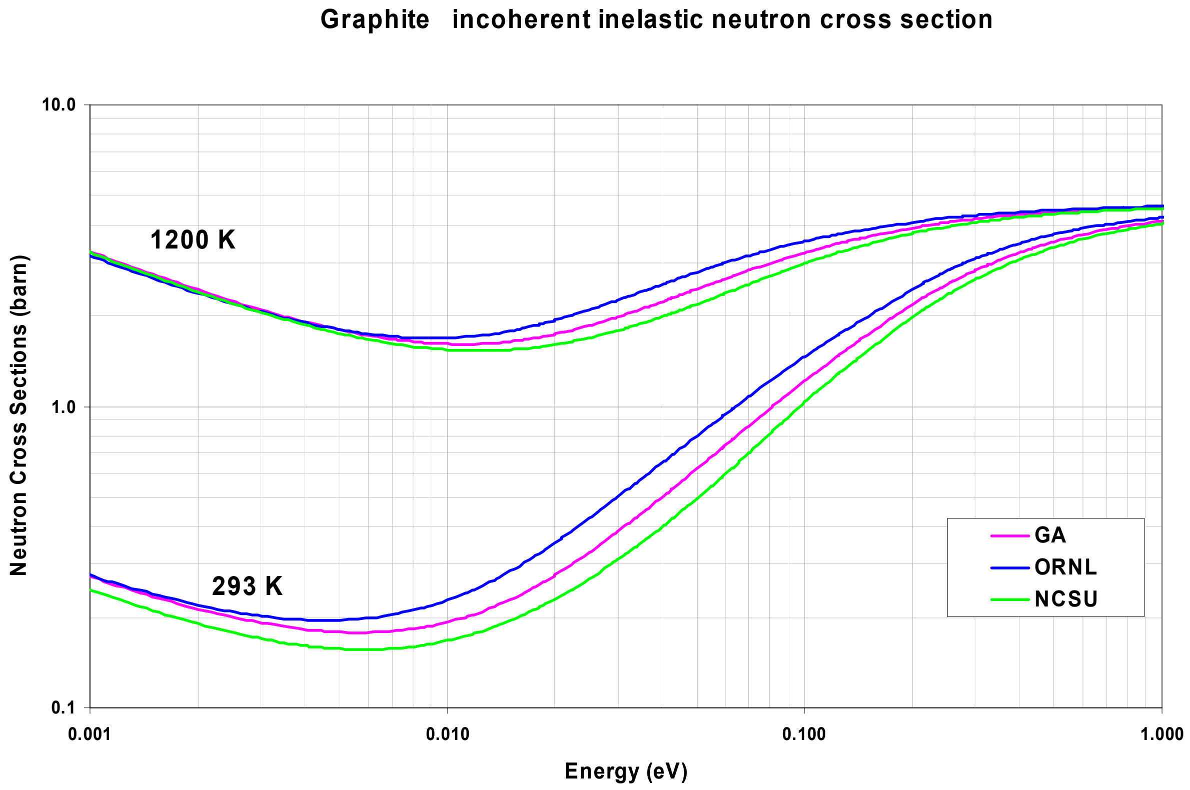

Fig. 39: Incoherent inelastic scattering cross section for graphite for GA, ORNL and NCSU model

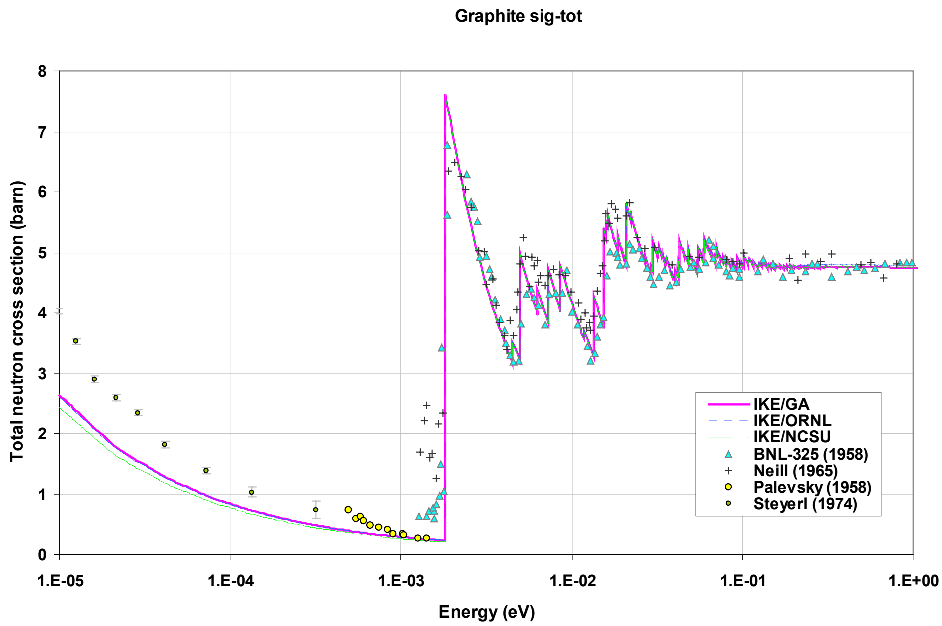

Total scattering cross section for graphite according to GA, ORNL and NCSU model

Fig. 40: Total scattering cross section for graphite according to GA, ORNL and NCSU model

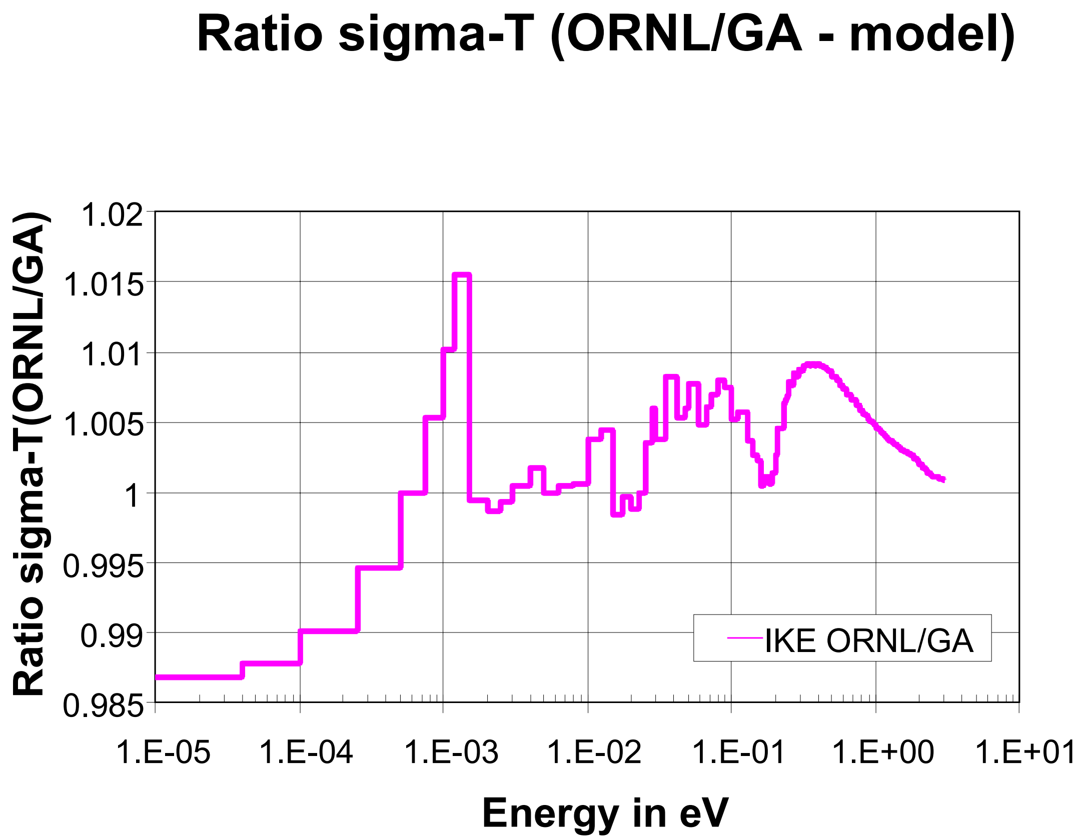

Fig. 41: Ratio of total cross section for graphite (ORNL vs GA model)

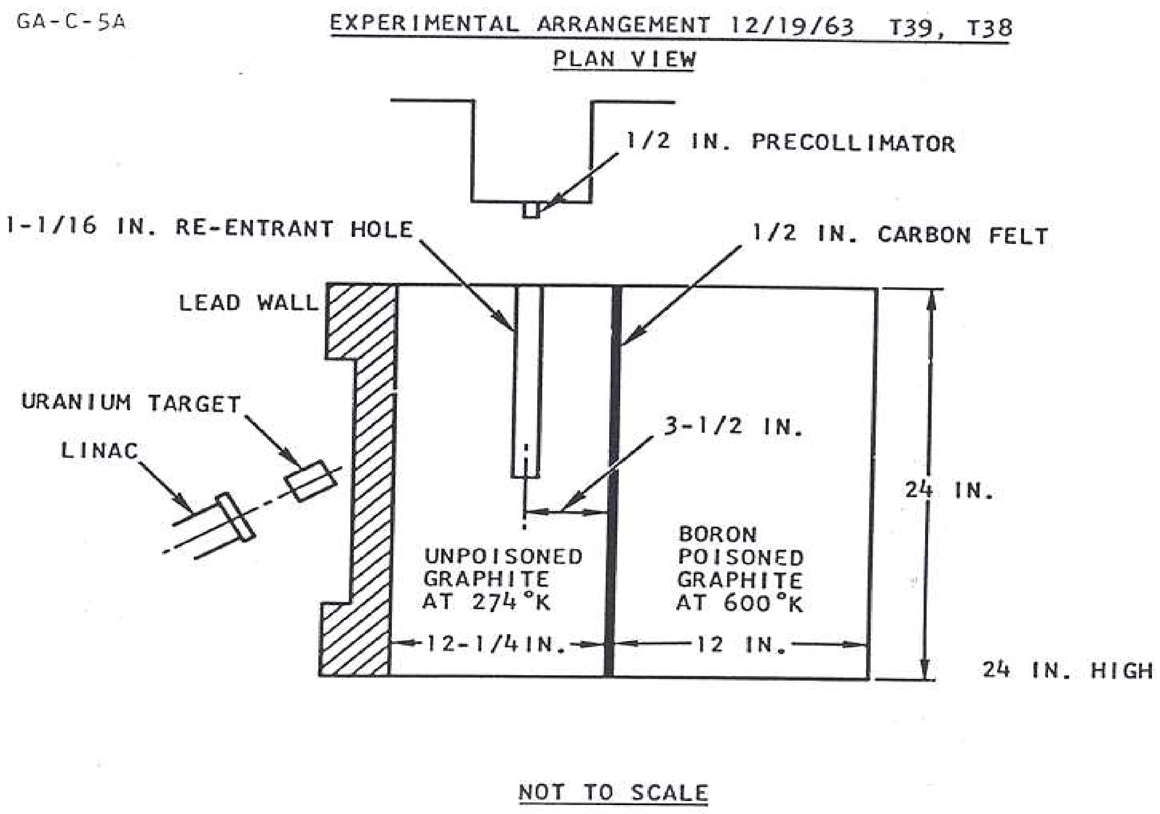

Fig. 42: Experimental arrangement for measuring neutron spectra in unpoisoned graphite

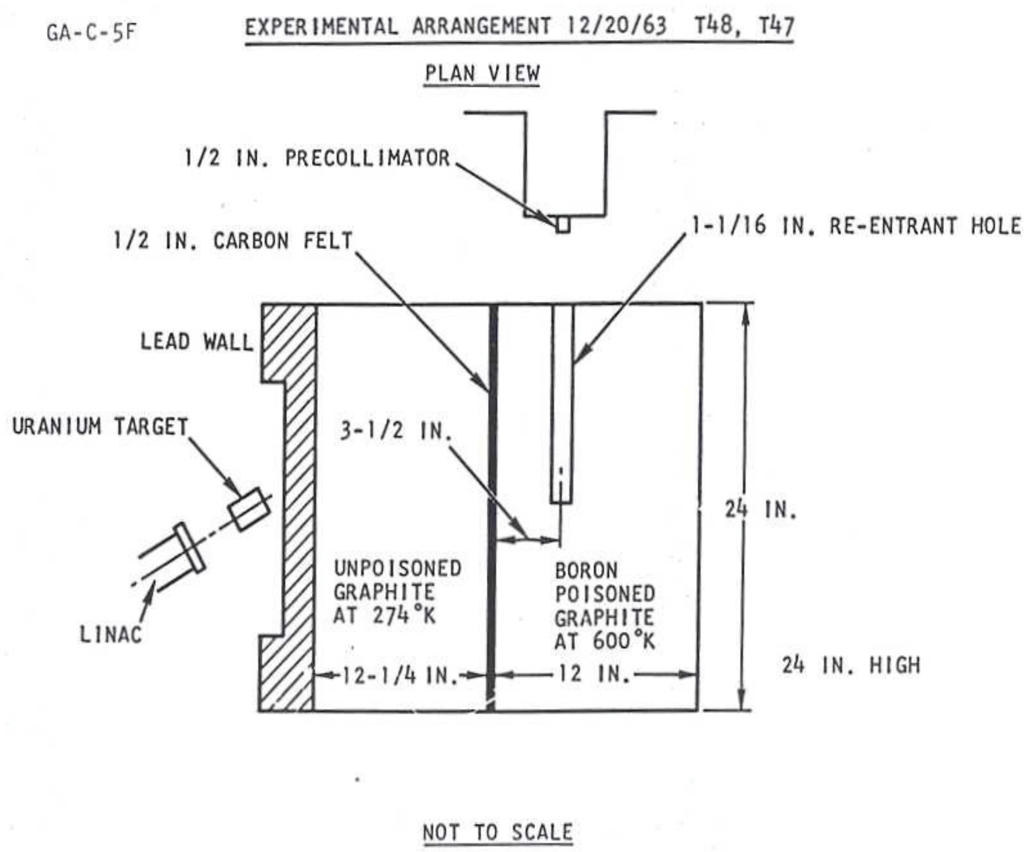

Fig. 43: Experimental arrangement for measuring neutron spectra in boron poisoned graphite

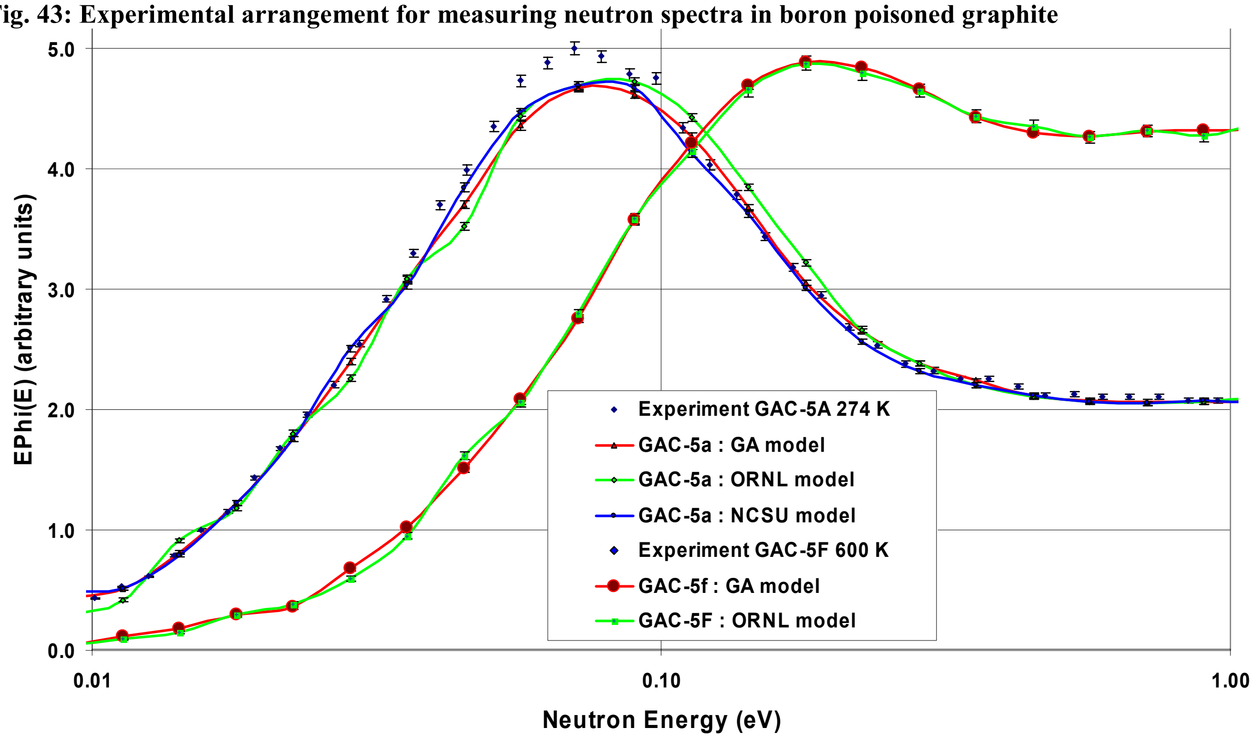

Fig. 44: Measured neutron spectra in poisoned and unpoisoned graphite compared with calculations based on different scattering law models

90 Degree angular neutron spectrum in samarium poisoned graphite at 600K

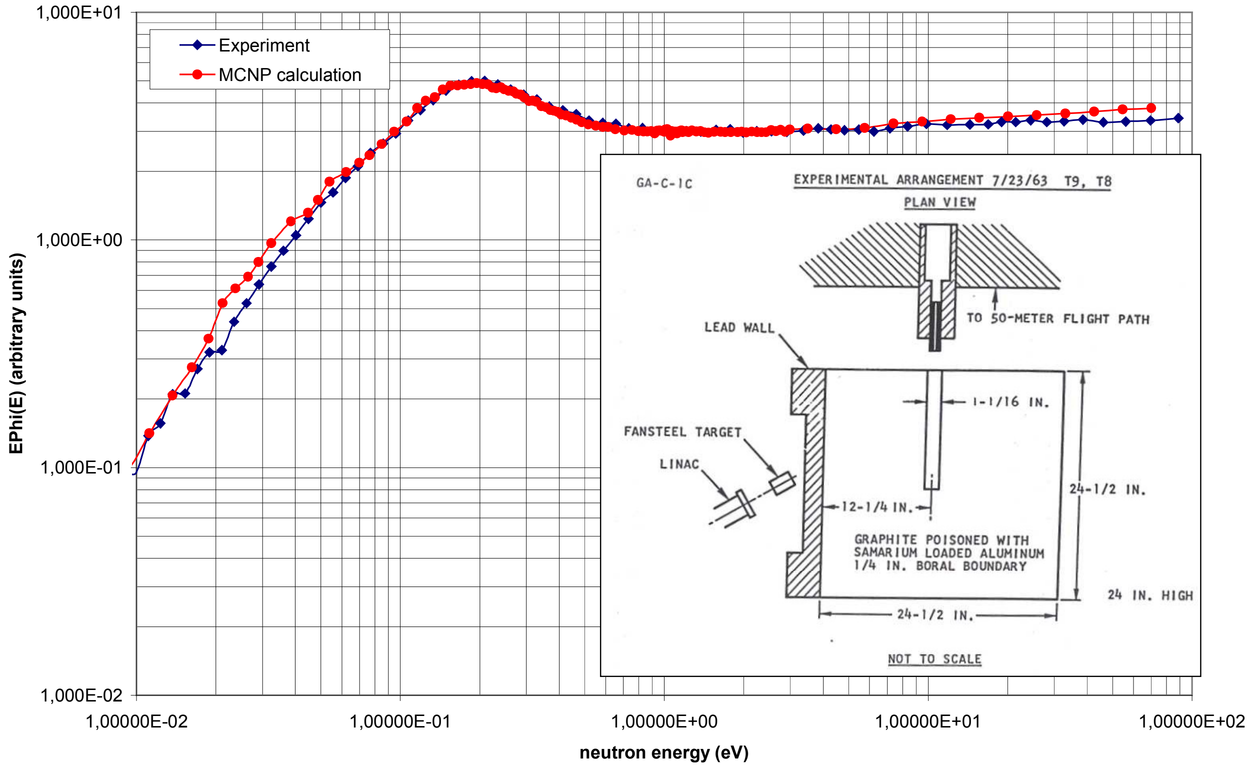

Fig. 45: 90 Degree angular neutron spectrum in samarium poisoned graphite at 600 K

Neutron flux density spectra for the graphite Benchmark GA-C-1B

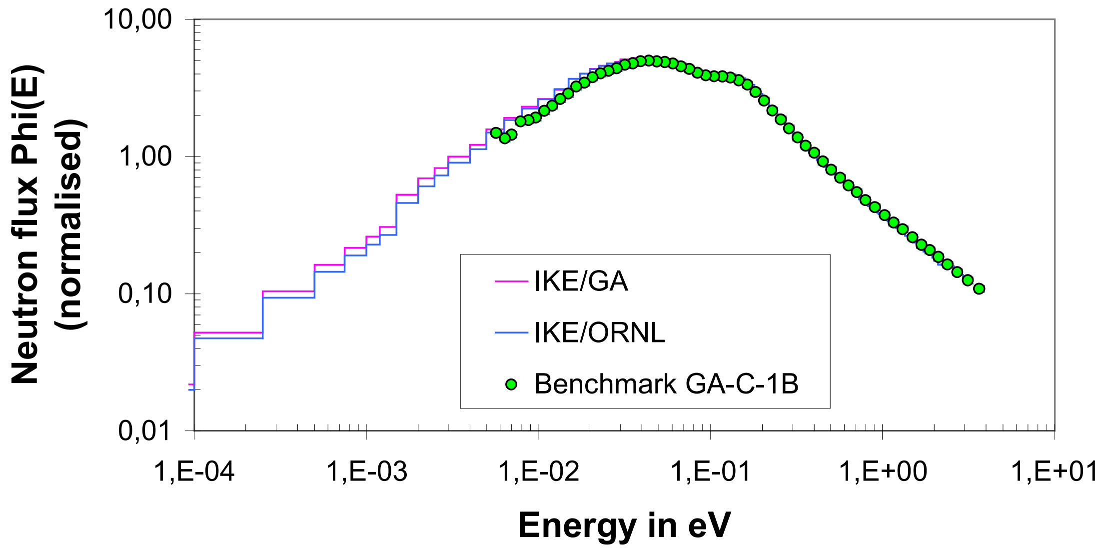

Fig. 46: Neutron flux density spectra for the graphite benchmark GAC-1B

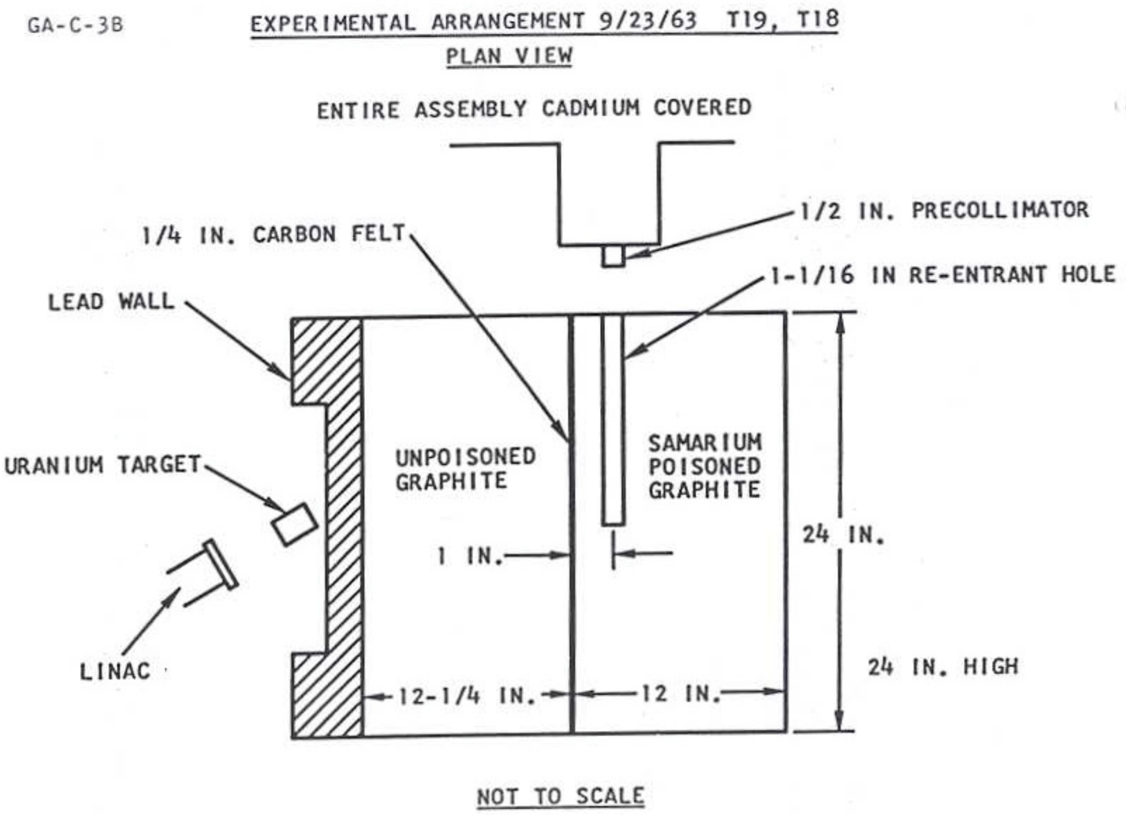

Fig. 47: Experimental arrangement for measurment of neutron spectra in graphite

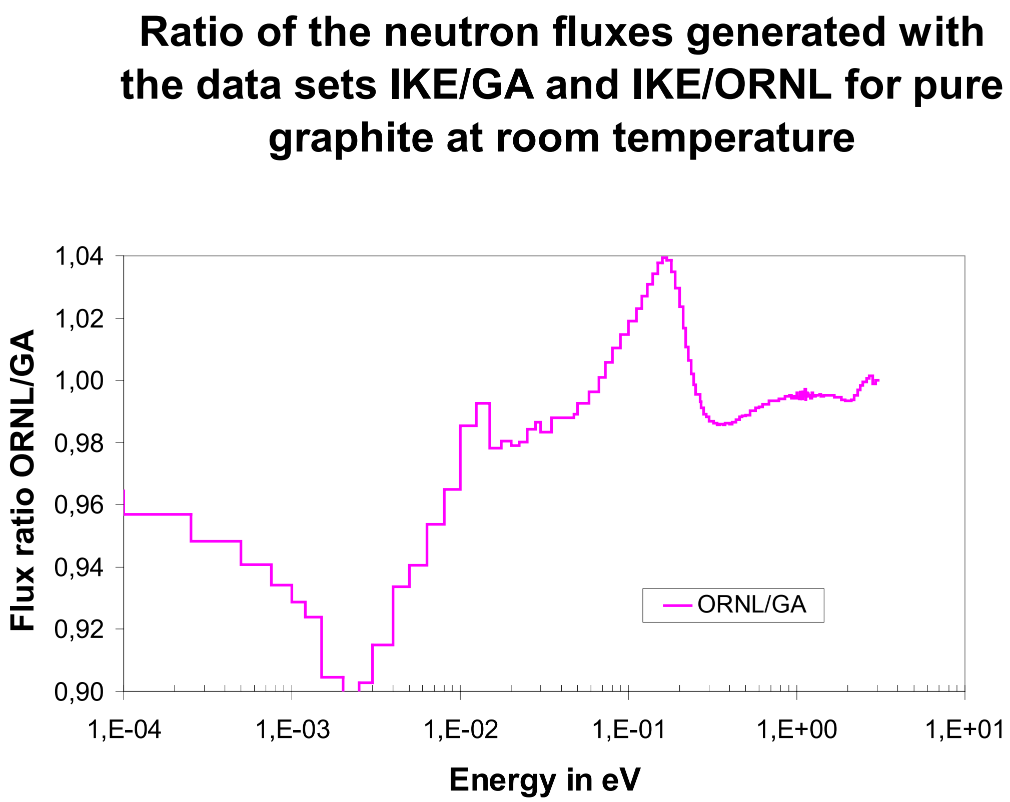

Fig. 48: Ratio of neutron spectra in pure graphite at room temperature (ORNL vs GA model)

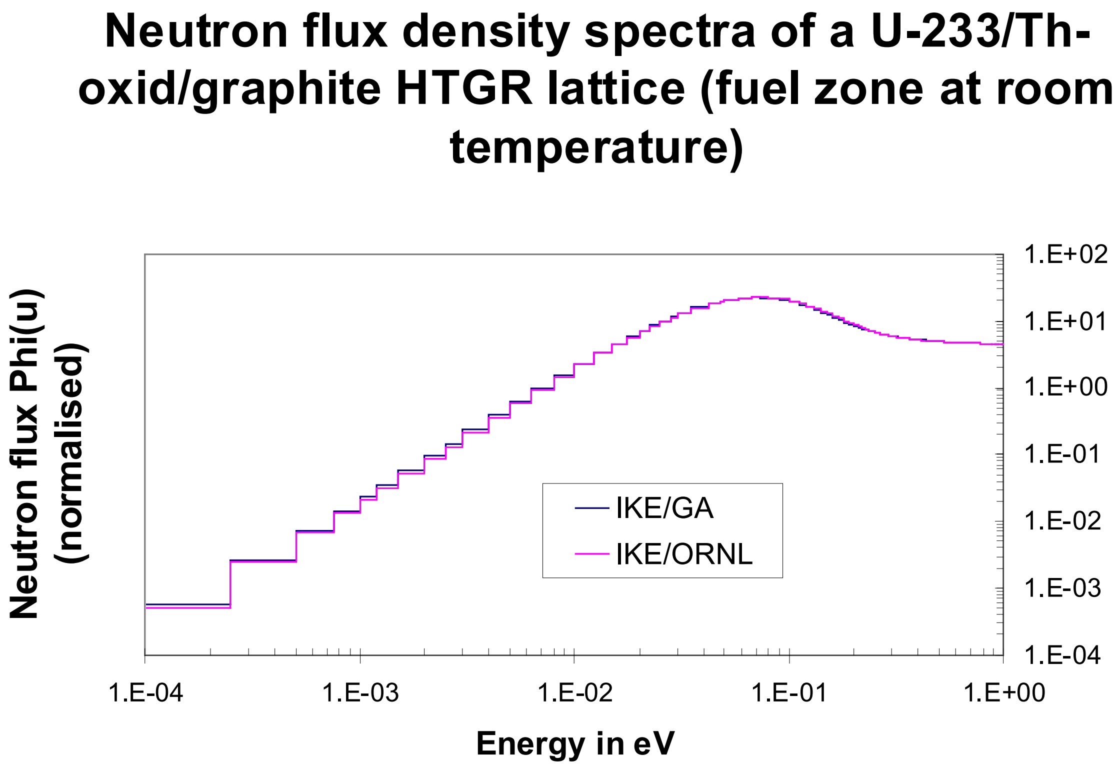

Fig. 49: Neutron flux density fuel zone spetra for a graphite moderated U-233/Th lattice at 293 K (ORNL and GA model)

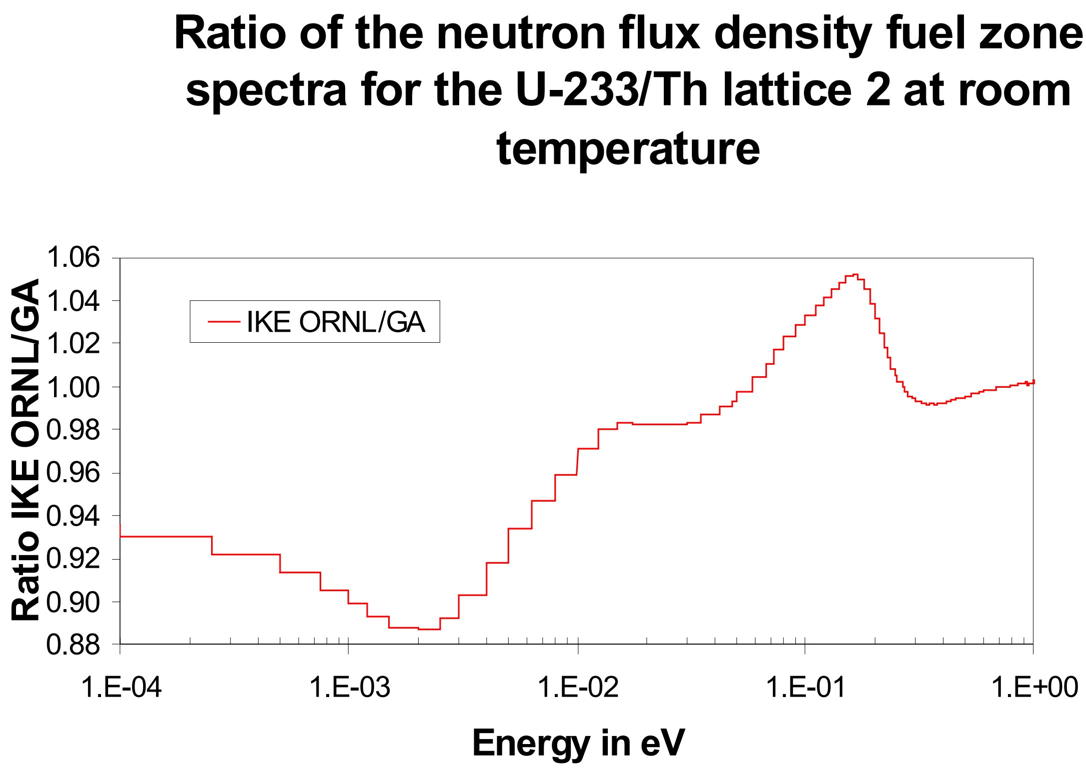

Fig. 50 Ratio of the neutron flux density fuel zone spetra for a graphite moderated U-233/Th lattice at 293 K (ORNL vs GA model)

Neutron flux density spectra of a U-233/Th-oxid/graphite HTGR lattice (fuel zone at 1023K)

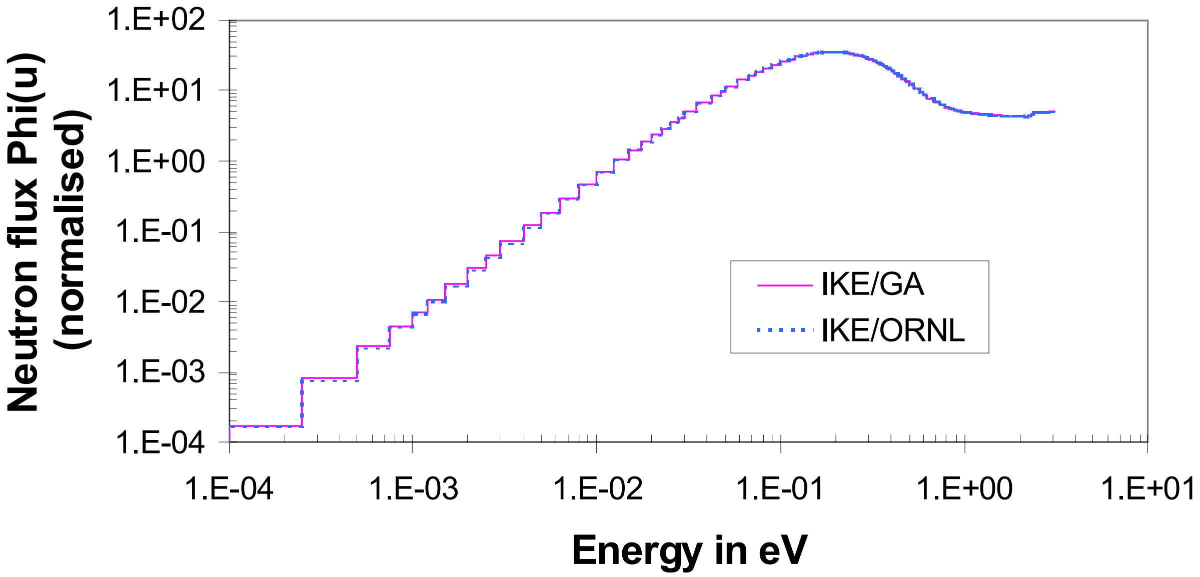

Fig. 51: Neutron flux density fuel zone spetra for a graphite moderated U-233/Th lattice at 1023 K (ORNL and GA model)

Ratio of the neutron flux density fuel zone spectra for the U-233/Th lattice 2 at 1023K

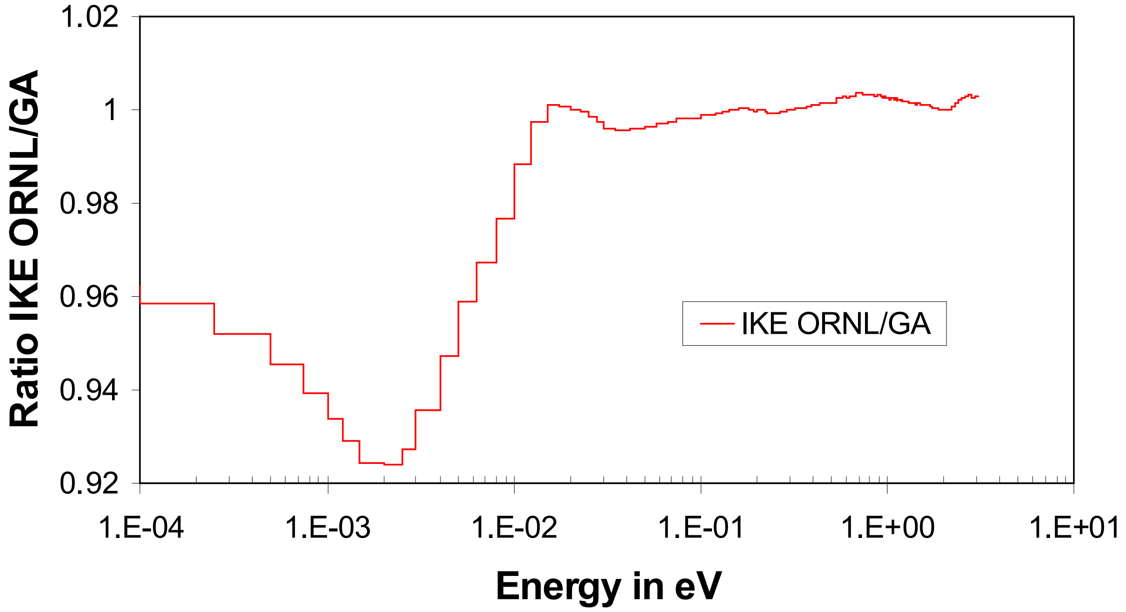

Fig. 52: Ratio of the neutron flux density fuel zone spetra for a graphite moderated U-233/Th lattice at 1023 K (ORNL vs GA model)

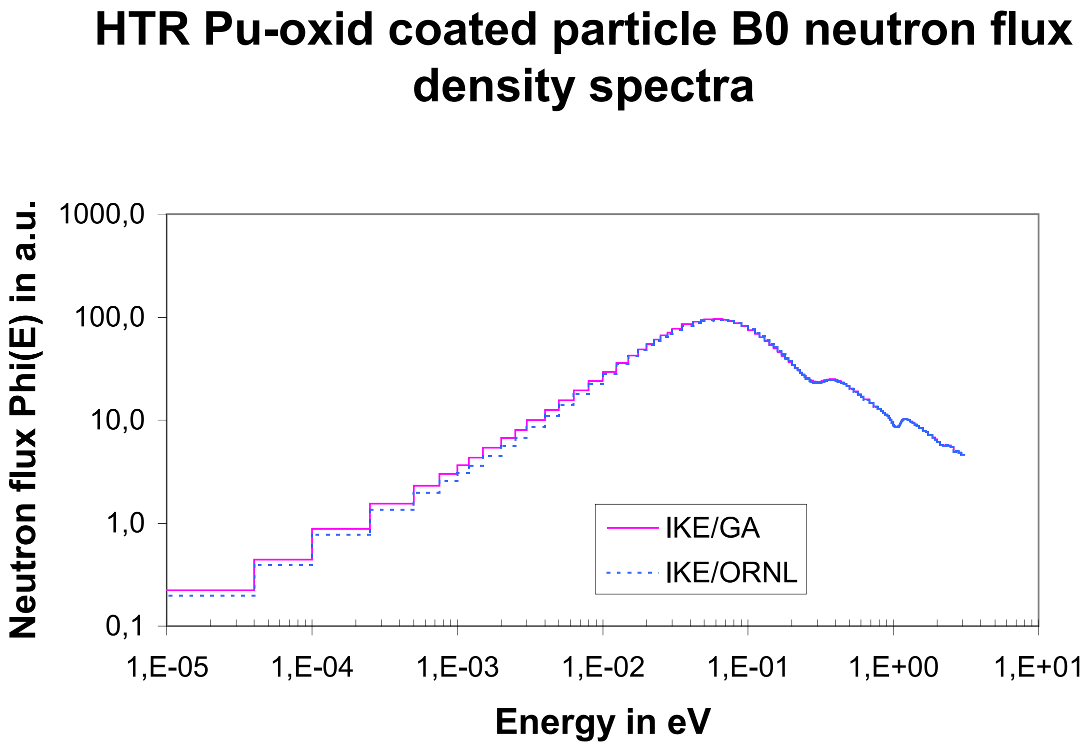

Fig. 53: Average neutron flux density in a HTR Pu oxide coated particle cell (ORNL and GA model)

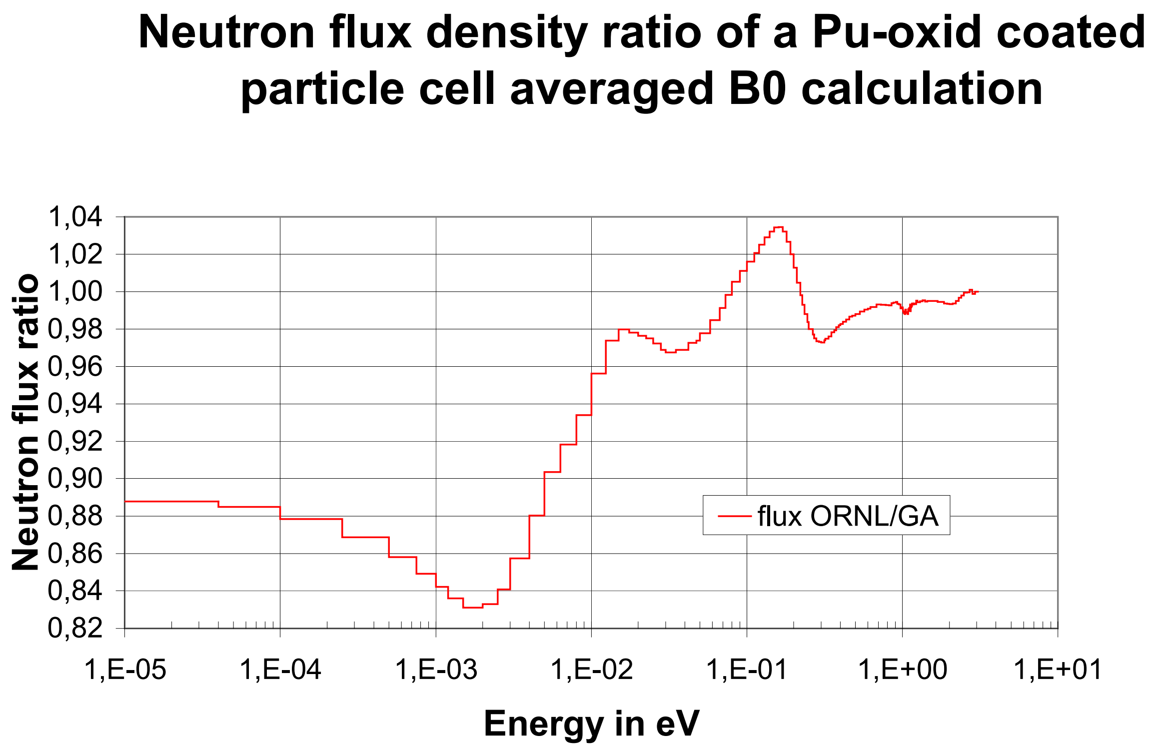

Fig. 54: Average neutron flux density ratio in a HTR Pu oxide coated particle cell (ORNL vs GA model)

HTR Pu-oxid coated particle fuel zone neutron flux density spectra

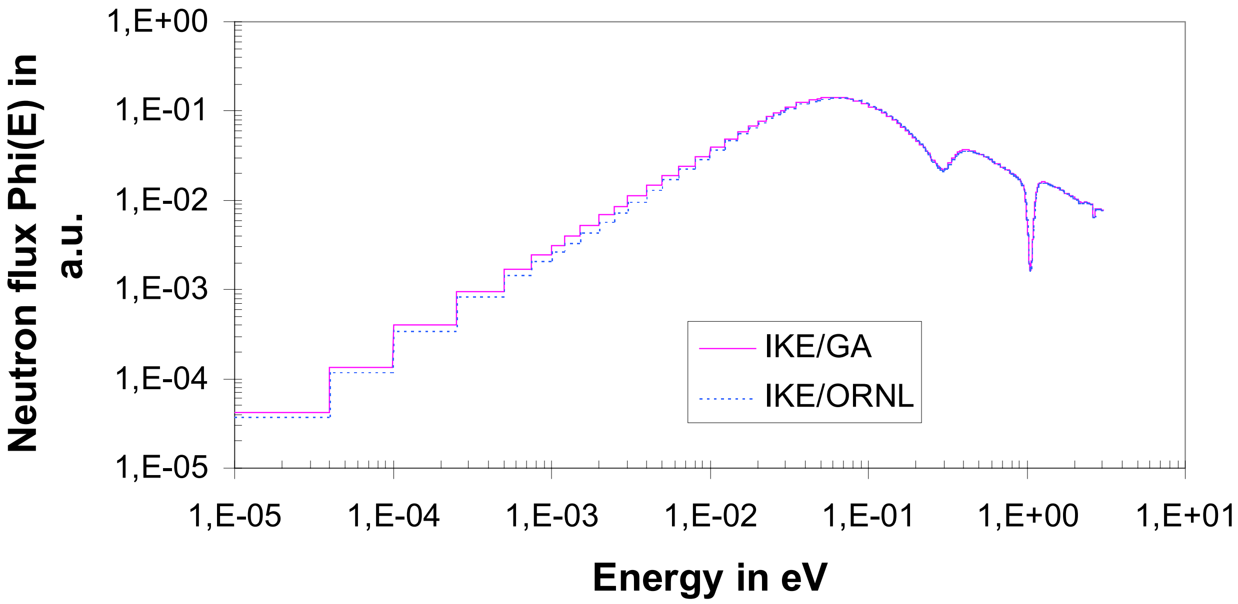

Fig. 55: Central neutron flux density in a HTR Pu oxide coated particle (ORNL and GA model)

Neutron flux density ratio in the Pu-oxid coated particle fuel zone

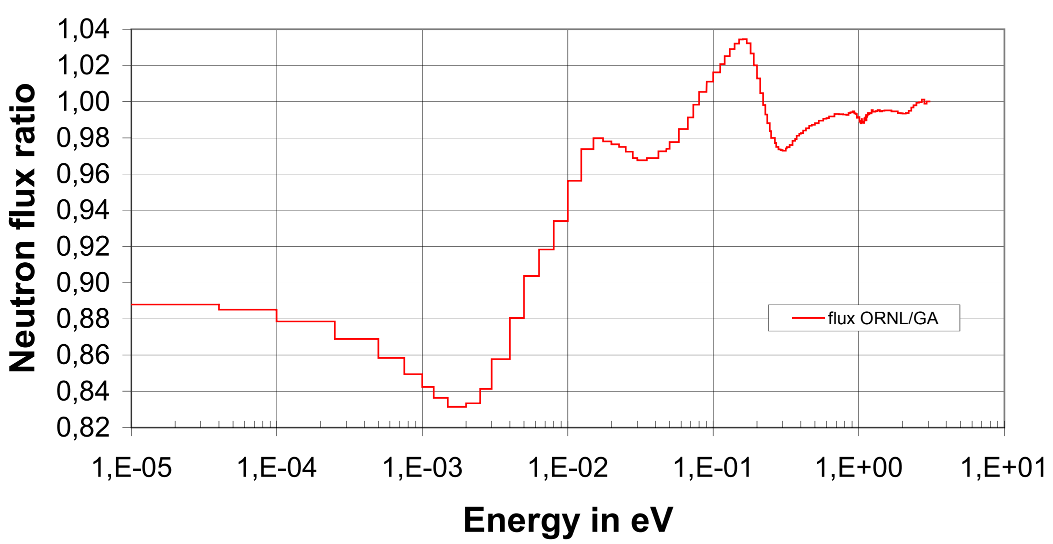

Fig. 56: Central neutron flux density ratio in a HTR Pu oxide coated particle (ORNL vs GA model)

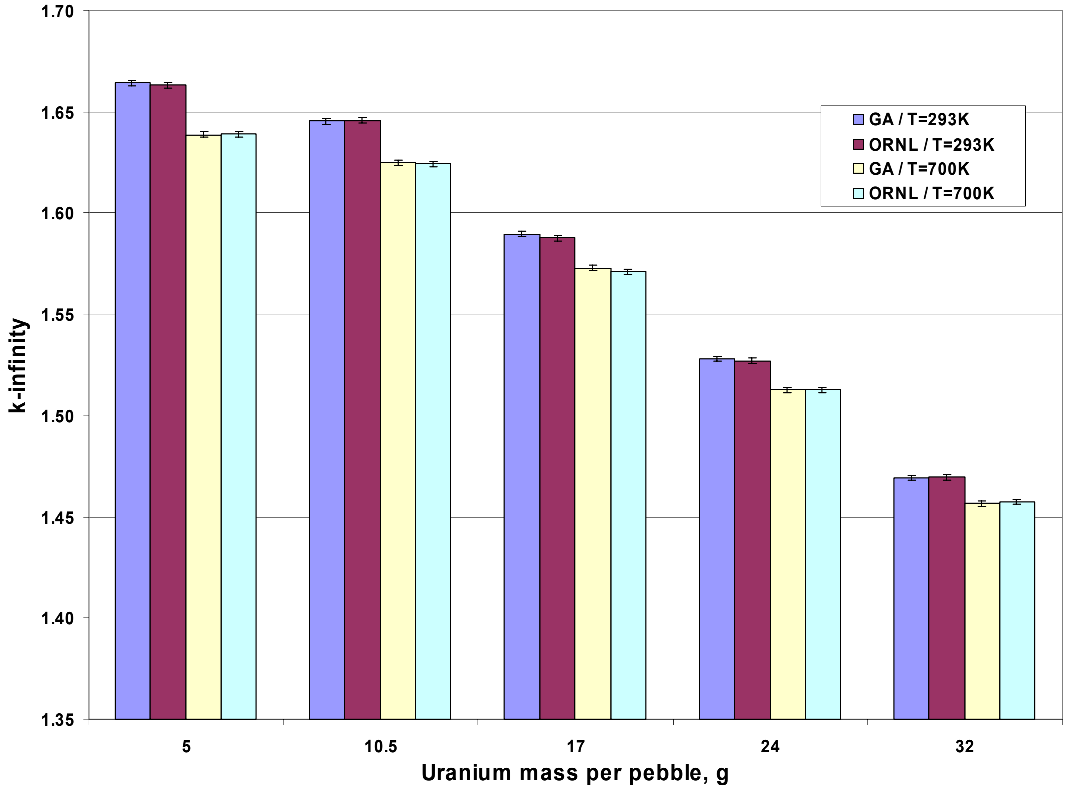

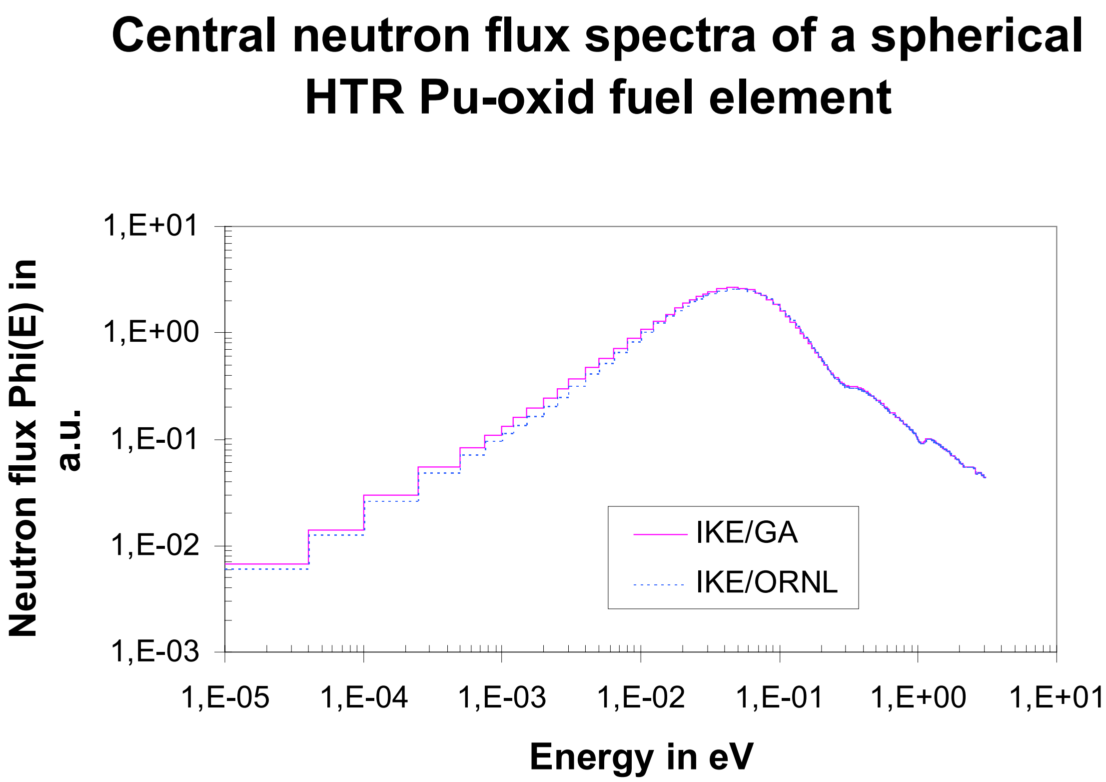

Fig. 57: Central neutron flux density in a HTR spherical fuel element (ORNL and GA model)

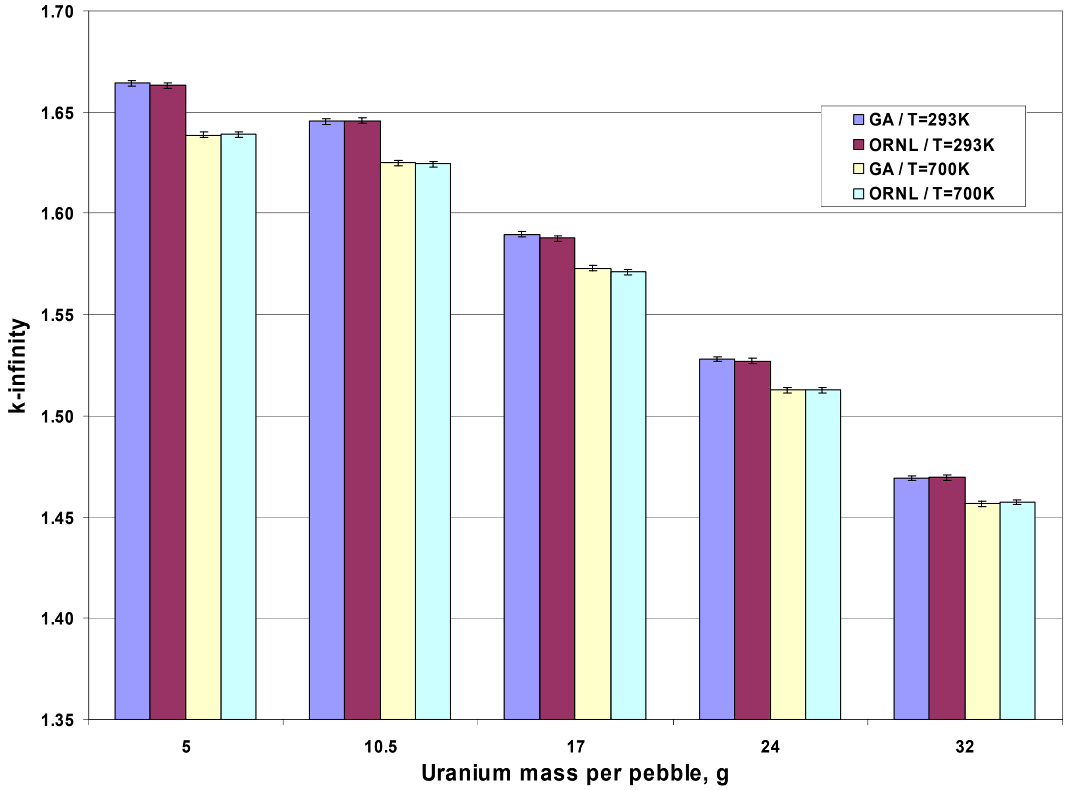

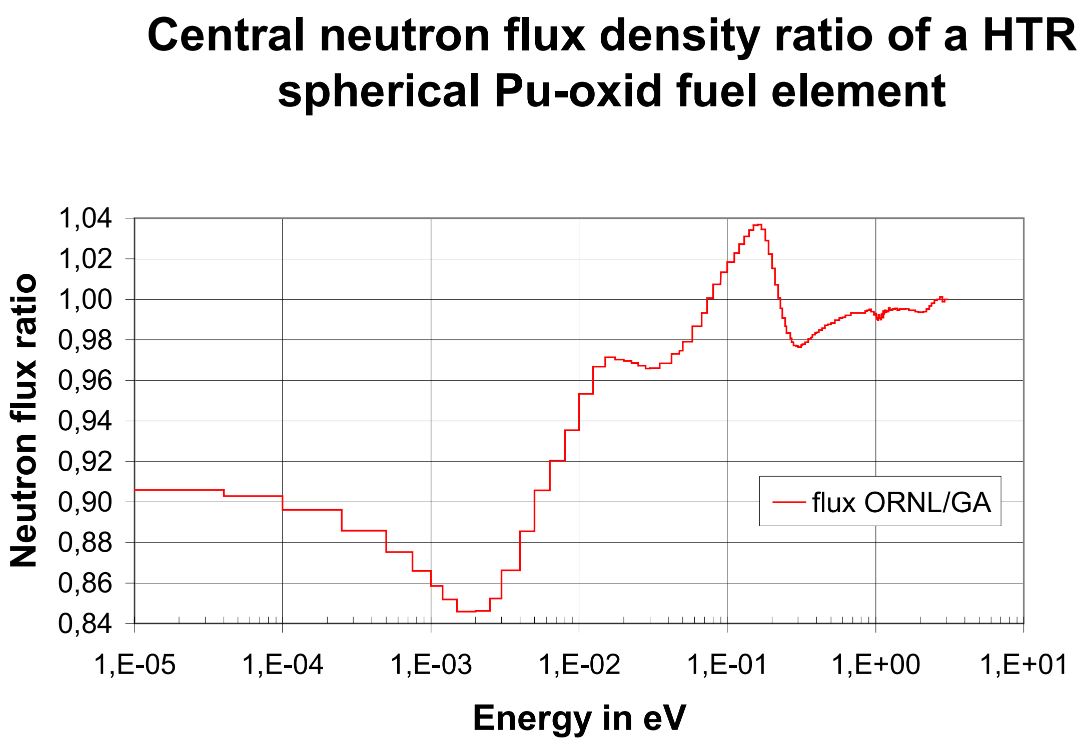

Fig. 58: Central neutron flux density ratio in a HTR spherical fuel element (ORNL vs GA model)

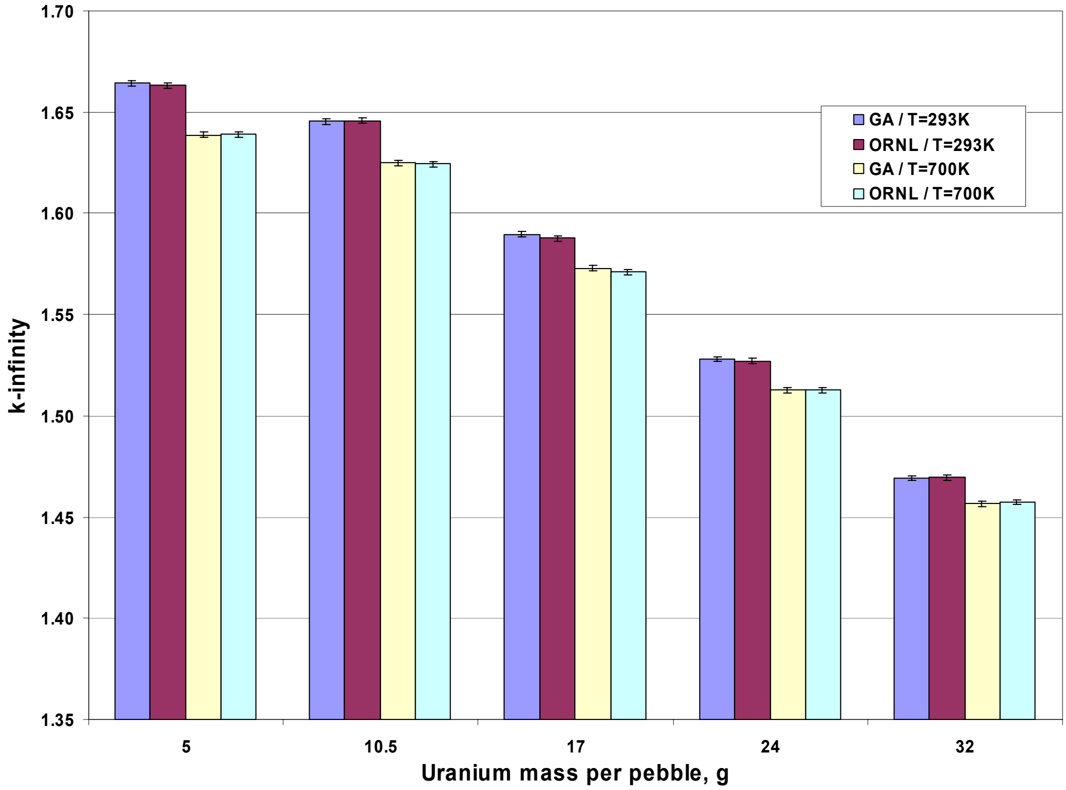

Fig. 59 K-inf as a function of U mass per HTR pebble for 293K and 700K according to ORNL and GA scattering model (MCNP-calculations)

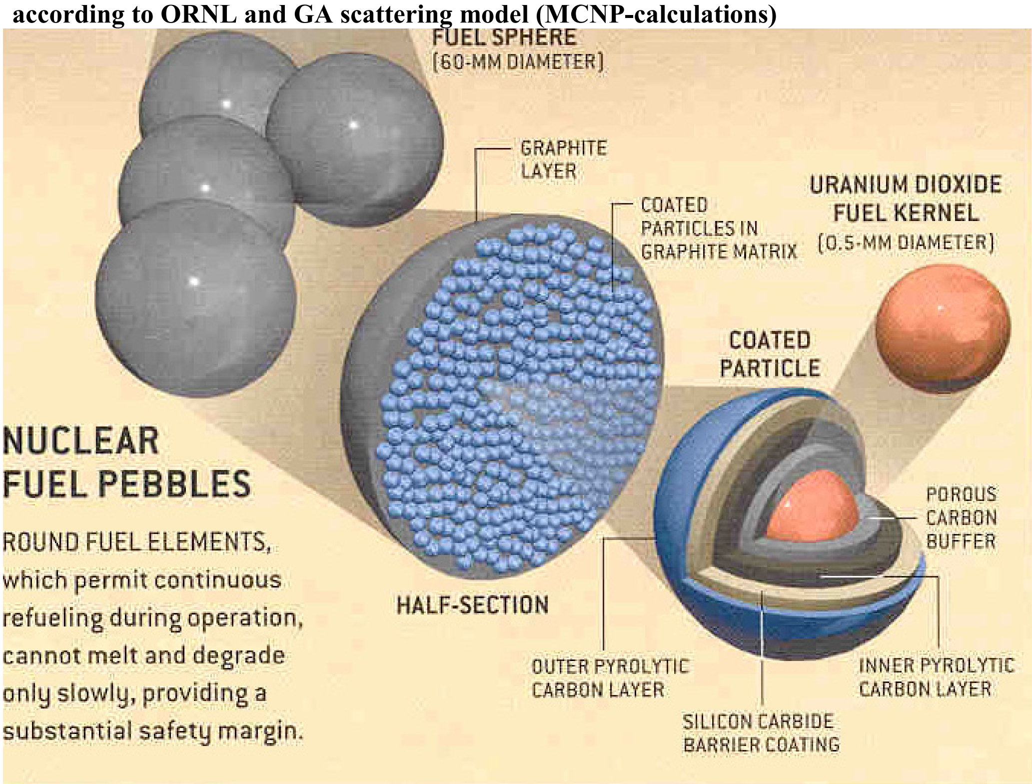

Fig. 60: Pebble fuel element with coated particles